Sensory conflict disrupts circadian rhythms in the sea anemone *Nematostella vectensis*

Cory A. Berger[1,2], Ann M. Tarrant[1*]

1 Biology Department, Woods Hole Oceanographic Institution, Woods Hole, MA 02543, United States

2 MIT-WHOI Joint Program in Oceanography/Applied Ocean Science & Engineering, Cambridge and Woods Hole, MA, USA

* atarrant@whoi.edu

Abstract

Circadian clocks allow organisms to optimize their phenotypes in relation to rhythmic environmental conditions. Clocks must synchronize, or entrain, to environmental signals called zeitgebers (such as light and temperature) while maintaining internal rhythms that are robust to environmental noise. We know surprisingly little about how clocks function in the presence of multiple zeitgebers, although these are the conditions that exist in nature. Misalignment between zeitgeber cycles (here, "sensory conflict") can disrupt circadian rhythms in behavior and gene expression, but it is not clear whether this is generally true across animals. In order to understand general rules about animal clocks, and how clocks have evolved throughout Metazoa, it is necessary to study non-bilaterian animals such as cnidarians, which include corals, jellies, and sea anemones. The sea anemone *Nematostella vectensis* has emerged as the principal model system for cnidarian circadian biology. In this study, we show that temperature cycles entrain circadian locomotor rhythms in *Nematostella*, and then conduct extensive behavioral experiments across a range of light and temperature cycles to show that *Nematostella*'s circadian behavior is disrupted by sensory conflict. Chronic exposure to conflicting light and temperature cycles also causes substantial changes to the rhythmic transcriptome, including the breakdown of rhythmic expression of various metabolic processes. These results have important implications for our understanding of cnidarian circadian

clocks at both the molecular and organismal levels, and for how sensory information is processed by clocks in the absence of a central nervous system.

Introduction

Nearly all organisms use circadian clocks to synchronize their behavior, physiology, and metabolism to ∼24h environmental cycles. These endogenous molecular timekeepers integrate information from environmental signals called zeitgebers, which include light, temperature, and food availability. Zeitgebers entrain endogenous rhythms, and can also directly drive rhythmic behavior or gene expression. Rhythmic behavior is thus the result of both endogenous (circadian) and exogenous (zeitgeber-driven) signals, leading to potentially complex behavioral outcomes. For instance, direct effects of environmental cues can mask endogenous rhythms [1], and, conversely, circadian rhythms can constrain or "gate" acute environmental responses [2, 3]. Zeitgebers can also provide conflicting information to the clock, a situation called "sensory conflict," and potentially disrupt circadian rhythms [4]. Understanding how environmental information is transmitted into rhythmic behavior is a central goal of circadian biology, but we know very little about how clocks integrate information from multiple zeitgebers (reviewed for insects in [5, 6]).

Although light is the best-studied zeitgeber, temperature cycles also provide a nearly-universal entraining cue for circadian rhythms. Ambient temperature cycles have been shown to entrain the clocks of bacteria [7, 8], non-metazoan eukaryotes [9, 10], arthropods [11–14], vertebrates [15, 16], and recently even homeothermic mammals [17]. No studies have yet investigated thermal entrainment in non-bilaterian animals, and few studies have measured circadian behavior during simultaneous light and temperature cycles in any animal. Since the late 1950's, there have been studies of conflicting light and temperature cycles in insects [4, 18–24], vertebrates [25–28], protists [29], and cyanobacteria [30]. There have also been studies of light in conjunction with time-restricted feeding in vertebrates [31–34]. However, most of these studies did not compare more than two possible phase relationships between zeitgebers, precluding characterization of the potentially non-linear relationship between an entrained rhythm and two entraining cues. If any generalization can be made from this literature, it is that circadian behavior may preferentially entrain to a single zeitgeber under certain conditions, while under other conditions, behavior might display an intermediate relationship or be disrupted in some way. There is a need for studies that comprehensively test multiple phase relationships between zeitgebers in order to understand the conditions under which

"normal" clock output is possible, when clock function is disrupted, and how such properties of the clock generalize to different taxonomic groups.

Cnidaria, a diverse phylum that is likely sister to Bilateria [35] (but see [36]), has the best-studied circadian rhythms among non-bilaterian animals and represents an important group in which to address these questions. The sea anemone *Nematostella vectensis*, the principal model system for circadian rhythms in Cnidaria, exhibits nocturnal rhythms in locomotion that entrain to artificial light-dark cycles [37,38] and to natural environmental conditions [39]. While behavioral rhythms in *Nematostella* and other anthozoans persist in constant or "free-running" conditions, they have been described as "weak" in the sense that they are less persistent and more variable among individuals compared to vertebrates or *Drosophila* [40]. For example, *Nematostella*'s behavioral rhythms attenuate after a few days in constant darkness [38], and a large portion of gene expression rhythms appear not to free-run [41, 42]. Cnidarians also fundamentally differ from bilaterians in that they lack a central nervous system. A distinction is often drawn between central clocks in the brain and peripheral clocks in other tissues, with the central clock acting to synchronize peripheral clocks [43]. Certain phase relationships between light and temperature cycles cause arrythmic locomotor behavior and disruption of the central clock in *Drosophila* [4], but not of peripheral clocks, which preferentially entrain to light [22]. This raises the possibility that behavioral disruptions under sensory conflict are caused by differential entrainment of central and peripheral clocks. Cnidarians by definition lack this distinction and thus provide an important system in which to study sensory conflict.

The most proximal function of circadian clocks is to regulate transcription through the activity of circadian transcription factors. Animal clocks consist of transcription-translation feedback loops (TTFLs) in which these transcription factors activate the expression of their own repressors, as well as other downstream genes that may be cell- or tissue-specific. The molecular architecture of circadian TTFLs is understood in model systems within Bilateria, but is largely unknown in Cnidaria. Some genes involved in bilaterian TTFLs are conserved in cnidarians, including the basic-helix-loop-helix-per-arnt-sim (bHLH-PAS) transcription factors Clock (CLK) and Cycle (CYC), which activate circadian gene expression in both vertebrates and *Drosophila* (reviewed in [44] and [45]). Dimerization between *Nematostella* CLK and CYC has been shown *in vitro* [41], supporting the hypothesis that their role in the circadian clock is conserved. However, cnidarians lack orthologs of Period, which is the main repressor of vertebrate CLK/CYC [40, 46] (in conjunction with Timeless in vertebrates and Cryptochrome in *Drosophila* [44, 45]). This suggests that there are major differences in clock

architecture between bilaterians and cnidarians. *Nematostella* possesses several cryptochromes, one of which is homologous to a mammalian repressor of CLK (Cry2), and others of which belong to an anthozoan-specific clade [47]. Several other genes have received attention as possible circadian regulators because they show robust diel oscillations in gene expression in *Nematostella* and other anthozoans. These include an ortholog of CIPC, which is a negative regulator of mammalian Clock activity [48], as well as Helt-like (Helt; a bHLH transcription factor) and two proline and acidic amino acid-rich bZIP (PAR-bZIP) transcription factors [38, 49].

Circadian regulation of gene expression, in combination with direct responses to zeitgebers, ultimately produces organismal rhythms in behavior and physiology. It is therefore necessary to relate behavior, core clock gene expression, and the expression of downstream genes with one another in order to understand how circadian rhythms are affected by conflicting zeitgeber regimes. Although previous studies in insects have measured the expression of individual clock genes during sensory conflict [23], or transcriptome-wide patterns of gene expression under aligned light and temperature cycles [50], we are not aware of any study that has examined the transcriptome under conflicting light and temperature cycles. Thus, the extent to which global patterns of gene expression are affected by sensory conflict is unknown.

In the current study, we show that temperature cycles drive circadian behavior in *Nematostella*, producing activity profiles similar to light-driven rhythms. We then comprehensively test different combinations of light and temperature cycles and show that aligned cycles drive normal rhythmic behavior, while behavior becomes arrhythmic under large degrees of sensory conflict. This includes the disruption of free-running rhythms, indicating changes to the endogenous clock itself. Having shown that sensory conflict disrupts circadian behavior in *Nematostella*, we then profile transcriptome expression during sensory conflict in order to characterize global changes in rhythmic gene expression that underlie disrupted behavior. We find that sensory conflict causes substantial, chronic changes to diel gene expression, including the loss and gain of rhythmic genes, phase shifts, and disruption of co-expressed gene modules related to cellular metabolism. This study extends our understanding of temperature entrainment and integration of multiple zeitgebers to a non-bilaterian model animal, sheds light on the molecular and physiological changes that underpin behavior disruptions resulting from sensory conflict, and informs our understanding of how environmental signals contribute to rhythmic behavior at the organismal level.

Results

Temperature cycles drive circadian rhythms in *Nematostella*

Anemones maintained in constant darkness with a temperature cycle that changed gradually from 14–26 °C (1 degree per hour; Fig. 1a) exhibited rhythmic diel behavior (n = 18, eJTK test, $p = 3e-5$; LSP permutation test, $p < 0.001$, Fig. 2a). Peak activity occurred at ZT18, 6h after the onset of cooling (ZT0 is the coldest point of the cycle). There were 10/18 individuals (56%) with a significant 24 h rhythm ($p < 0.001$), and their phases were clustered non-uniformly (Rayleigh test of circular uniformity, $p = 5e-4$) with a mean phase of 16.7, indicating phase synchronization among individuals (Fig. 2b). We observed similar results for a broader temperature cycle that changed from 8–32 °C (n=17, Fig. 2a).

We tested for the presence of free-running rhythms by transitioning anemones from the 14–26 °C temperature cycle to constant temperature (20 °C). The mean activity profile had a significant period between 20–28 h (LSP; $p < 0.001$, n=23), but did not have a significant period at exactly 24 h (eJTK, $p = 0.99$). There were 8/23 individuals (35%) that were rhythmic between 20–28 h (LSP, $p < 0.001$), and 4 individuals (17%) were rhythmic at 24 h (eJTK, p<0.001); if the mean behavior profile was re-calculated using only these 4 individuals, there was a significant 24h period (eJTK, p<0.001). Therefore, a subset of animals entrained circadian free-running behavior to the 14–26 °C temperature cycle. The mean behavior profile of anemones entrained to the 8–32 °C temperature cycle had a significant 24 h free-running rhythm (eJTK, $p = 6e-5$, n = 46), and 10/46 individuals (22%) had significant 24 h rhythms. Although these results may suggest that temperature is a weak entraining cue for *Nematostella*, the proportion of free-running individuals as determined by periodograms is comparable to anemones entrained to LD cycles in a previous study (35% vs. 33%) [39]. These results demonstrate that gradual, environmentally-relevant temperature cycles drive diel locomotor behavior and entrain circadian rhythms in *Nematostella*.

We used qRT-PCR to measure the expression of several core circadian genes (*Clock*, *Cry1a*, *Cry1b*, *Cry2*, and *Helt*) over 48 h of the 8–32 °C temperature cycle, and also during free-run. Only *Cry2* was rhythmic during the temperature cycle (LSP, $p < 0.001$), with peak expression at roughly ZT0 (Fig. 2c). No genes were rhythmic during free-run.

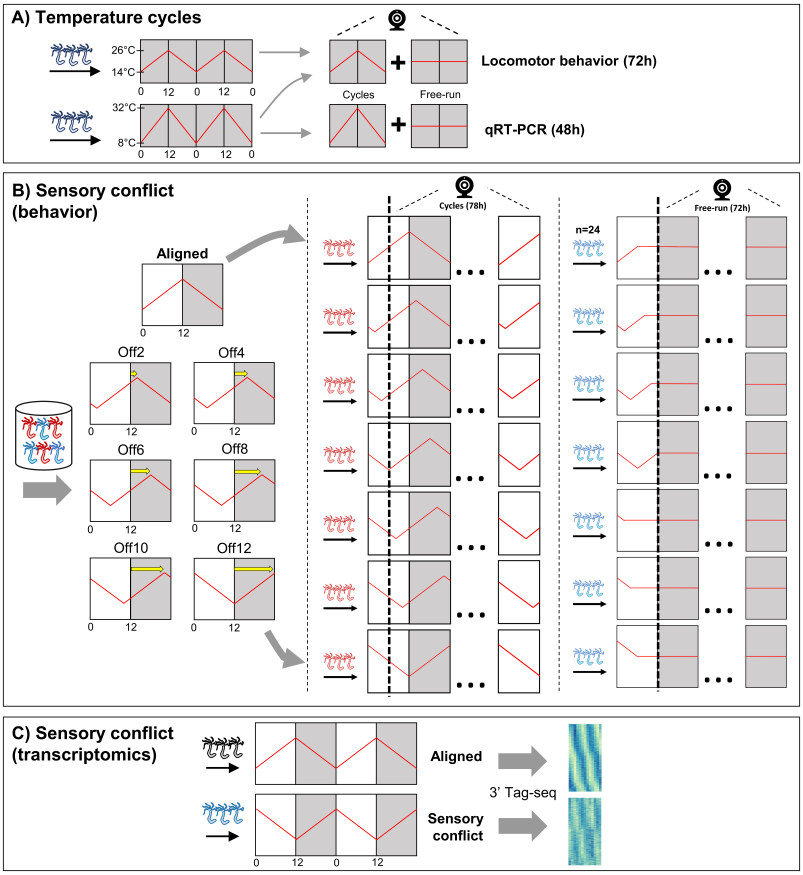

Figure 1. Schematic of the experimental design. A) Anemones in constant darkness were entrained to ramped temperature cycles that changed gradually from either 14–26 °C, or from 8–32 °C. ZT0 refers to the coldest time point. Locomotor behavior was recorded during cycling and free-running conditions for both cycles, and qRT-PCR was used to measure the expression of select clock-related genes for the 8–32 °C cycle. **B)** Animals were entrained to 12:12 b light-dark cycles and simultaneous 14–26 °C temperature cycles. In the Aligned (reference) group, the coldest part of the temperature cycle was aligned with lights-on; ZT0 always refers to lights-on. For 6 other groups of anemones, the phase of the temperature cycle was delayed relative to the light cycle in 2h increments up to 12h. Anemones were acclimated to experimental conditions for at least 2 weeks before measuring behavior. For each group, behavior was recorded for 78h during cycles (n=24[a]). Behavior was recorded for separate groups of anemones (n=24) for 72h during free-running (constant darkness, 20 °C). Shaded and unshaded regions represent dark and light periods, respectively. **C)** Gene expression was measured with 3'-anchored Tag-seq during Aligned light and temperature cycles, and 12h offset cycles. Anemones were sampled every 4h for 48h (13 time points) simultaneously for both time series. There were n=3 biological replicates at each time point, and each replicate consisted of 5 pooled individuals[b].

[a]Except 12h offset, which had n=36. [b]Except one library (at the 9th time point in the Aligned time series), which consisted of 3 pooled individuals

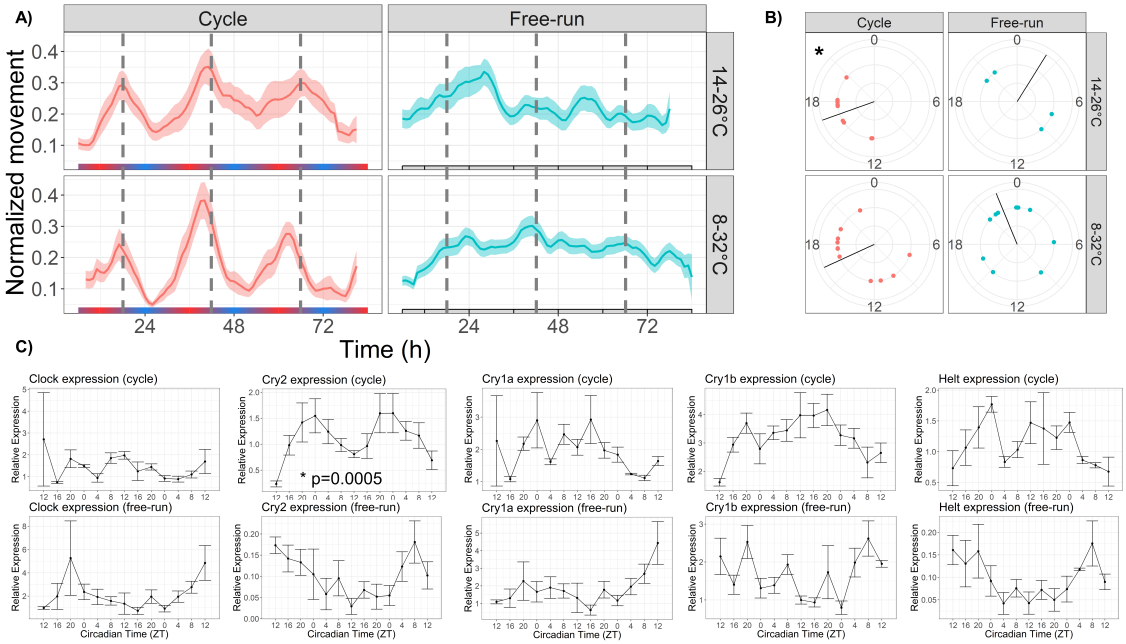

Figure 2. Temperature cycles drive rhythmic locomotor behavior, and weakly entrain circadian behavior. **A)** Mean behavior profiles of anemones in each group over 3 days. Individual locomotor profiles were normalized, averaged, and smoothed (see Methods). Shaded area represents standard error. Left, temperature cycles with scale bar indicating cold (blue) and hot (red) temperatures. Right, free-running at 20 °C. Dashed lines indicate ZT18, the period of peak activity during cycling conditions. **B)** Phases of rhythmic animals calculated by MFourFit. Black line represents circular mean. *:Rayleigh test, $p<0.05$. **C)** Expression of core circadian genes entrained to a temperature cycle and under free-running conditions. Only *Cry2* was significantly rhythmic (LSP, $p<0.05$).

Aligned light and temperature cycles entrain robust diel rhythms

We tested how the relationship between light and temperature cycles affects the circadian clock by acclimating groups of anemones to a gradually changing temperature cycle (14–26 °C) simultaneously with a 12:12 light-dark cycle. A schematic of the experimental design is shown in Fig. 1b. When light and temperature cycles were aligned such that lights-on corresponded to the coldest part of the temperature cycle (ZT0), *Nematostella* exhibited clear circadian behavior (Fig. 3a; eJTK p = 1.99E-05). Peak activity occurred at ZT19, during the middle of the dark phase; this is consistent with the phases of locomotor activity driven by light (ZT16-20, [37, 38]) and temperature cycles (ZT17-18, Fig. 2a). 20/24 individuals (83%) had significant 24h rhythms (eJTK, $p < 0.001$; Table 1), with a mean phase of 18.0 (Fig. 3b). Under free-run, the mean behavior profile also exhibited clear 24h rhythms (eJTK, $p < 0.001$) with peak activity at ZT12 (Table 2); 10/24 individuals (42%) had 24h rhythms, with a mean phase of 12.7. In summary, light and temperature cycles act synergistically to drive and entrain circadian behavioral rhythms in *Nematostella*.

Table 1. Summary statistics for sensory conflict experiments: **Cycling groups**

Group	LSP p-value[1]	LSP power	eJTK p-value[2]	n rhythmic[3]	Period[4]	Phase[4]	Mean phase[5]	Phase variance[6]	Amplitude[7]
Aligned-cycle	7.9e-4	0.85	2e-5	20/24	23.60	19.29	18.04	0.34	0.091
Off2-cycle	7.9e-4	0.75	2e-5	20/24	23.48	18.71	18.42	0.24	0.12
Off4-cycle	7.9e-4	0.84	2e-5	18/24	23.76	18.90	17.70	0.27	0.12
Off6-cycle	7.9e-4	0.60	2e-5	16/24	24.30	20.16	21.68	0.15	0.075
Off8-cycle	7.9e-4	0.85	2e-5	15/24	23.60	19.20	19.12	0.26	0.085
Off10-cycle	3.6e-3	0.19	1.7e-4	10/24	22.60	17.75	15.15	0.45	0.042*
Off12-cycle	7.9e-4	0.22	4.5e-3	13/36	23.66	18.62	13.29	0.86	0.015*

1) Tested periods between 20-28h; 2) Tested period of 24h; 3) eJTK $p<1 \times 10^{-3}$); 4) determined by MFourFit; 5) Circular mean of the phases of rhythmic individuals (eJTK $p<1 \times 10^{-3}$); 6) Circular variance of the phases of rhythmic individuals (eJTK $p<1 \times 10^{-3}$); 7) Determined with CircaCompare. *:Reduced amplitude compared to Aligned-cycle, CircaCompare, $p<0.05$. LSP: Lomb-Scargle periodogram

Table 2. Summary statistics for sensory conflict experiments: **Free-running groups**

Group	LSP p-value[1]	LSP power	eJTK p-value[2]	n rhythmic[3]	Period[4]	Phase[4]	Mean phase[5]	Phase variance[6]	Amplitude[7]
Aligned-FR	7.9e-4	0.47	7e-5	10/24	25.84	11.63	12.67	0.35	0.060
Off2-FR	7.9e-4	0.79	7e-5	6/24	22.62	16.50	18.28	0.63	0.071
Off4-FR	7.9e-4	0.51	7e-5	11/24	23.64	14.17	6.98	0.74	0.050
Off6-FR	0.13	0.095	0.76	5/24	27.34	18.57	3.50	0.73	4.9e-3*
Off8-FR	7.9e-4	0.67	7e-5	11/24	21.74	15.53	13.65	0.51	0.048
Off10-FR	0.53	0.042	0.61	7/24	28.00	3.39	10.78	0.70	2.8e-3*
Off12-FR	7.9e-4	0.32	7e-5	6/24	22.96	11.72	20.65	0.80	0.034*

1) Tested periods between 20-28h; 2) Tested period of 24h; 3) eJTK $p<1 \times 10^{-3}$); 4) determined by MFourFit; 5) Circular mean of the phases of rhythmic individuals (eJTK $p<1 \times 10^{-3}$); 6) Circular variance of the phases of rhythmic individuals (eJTK $p<1 \times 10^{-3}$); 7) Determined with CircaCompare. *:Reduced amplitude compared to Aligned-FR, CircaCompare, $p<0.05$. LSP: Lomb-Scargle periodogram

Sensory conflict disrupts rhythmic behavior

We tested the effects of long-term entrainment to different light and temperature regimes by delaying the phase of the temperature cycle relative to the light cycle in 2h increments (Fig. 1b). This formed 6 additional regimes (2, 4, 6, 8, 10, and 12h offsets); anemones were transferred from aligned light and temperature cycles to one of these offset regimes and acclimated for a minimum of two weeks. Within each zeitgeber regime, we recorded the behavior of separate groups of animals during cycling and free-running conditions, resulting in a total of 14 experimental groups including aligned conditions. As examples, we use the following notation to refer to experimental groups: Off6-cycle refers to a 6h offset between light and temperature, recorded during the cycles; Off6-FR refers to behavior recorded during free-run. We quantified the strength of circadian rhythms using several metrics: the maximum power of Lomb-Scargle periodograms used to assess rhythmicity; the amplitude of mean time series; the number of individuals with significant 24h rhythms above a strict cutoff (eJTK $p < 0.001$); the relative synchronization (circular variance) of the phases of rhythmic individuals; and the difference in activity between light and dark phases.

Large degrees of sensory conflict profoundly disrupted rhythmic behavior. When the phase of the temperature cycle was delayed by 12h relative to the light cycle—the largest possible misalignment—the normal activity pattern was visibly disrupted (Fig. 3a) and 24-h rhythmicity was only weakly detectable in the mean behavior profile (eJTK, $p=4.5 \times 10^{-3}$; Table 1). Under these conditions (Off12-cycle), 13/36 individuals (36%) were rhythmic, but their phases could not be distinguished from a circular uniform distribution (Rayleigh test, p=0.8). Compared to Aligned-cycle, the power and amplitude of the mean time series were lower, there were fewer rhythmic individuals, and the variance of the phases of rhythmic individuals was larger (Table 1). The difference in activity between dark and light phases was also severely reduced compared to Aligned-cycle in terms of both time active (linear mixed effects model; LMM, $p=1 \times 10^{-4}$) and distance moved (LMM, $p=2 \times 10^{-4}$; Fig. 3c). Behavioral disruptions were also obvious in Off10-cycle, where *Nematostella* had weaker rhythms compared to Aligned-cycle by all of the above metrics (LSP power, n rhythmic indivduals, phase variance, amplitude), and lower dark:light activity ratio, LMM p=0.013), and the phase of the mean time series was advanced by 1.5 h (CircaCompare, $p=5 \times 10^{-5}$). The reduction in the light-dark activity ratio during Off10-cycle and Off12-cycle was specifically due to increased activity during lights-on (LMM, $p<0.05$), with no difference in activity during lights-off (LMM, $p>0.1$).

Weakened locotomor rhythms in the Off10-cycle and Off12-cycle groups were caused both by a weakening of the rhythms of individual animals, and a lack of synchronization between the remaining rhythmic individuals. The percentage of rhythmic individuals declined monotonically with increasing SC, from 83% in Aligned-cycle to 36% in Off12-cycle (Table 1), and the LSP powers of animals in Off10-cycle and Off12-cycle were lower than during Aligned-cycle (Dunn test, $p < 0.05$; Fig. B in S1 Appendix). In addition, the phases of rhythmic individuals in Off10-cycle and Off12-cycle had much larger variances than other groups and could not be distinguished from uniform distributions (Table 1; Rayleigh test, $p>0.05$). Thus, under severe sensory conflict, individual *Nematostella* were less likely to exhibit rhythmic behavior, and less likely for that behavior to synchronize with other individuals. Anemones exhibited robust diel behavior under smaller degrees of misalignment (0-8h; Fig. 3). The Off2-cycle, Off4-cycle, and Off8-cycle groups exhibited rhythms similar to those in aligned conditions, with no significant phase shifts or reductions in rhythm strength. The Off6-cycle group also showed 24-h rhythms, but the mean phase of rhythmic individuals was delayed by 3.6h relative to Aligned-cycle (Watson, p=0.0046), and the mean behavior profile was also delayed relative to Aligned-cycle (CircaCompare, $p=4 \times 10^{-5}$). There was also a marginally significant circatidal (10-14h) component in the Off6-cycle group (LSP, p=0.006), and the dark:light activity

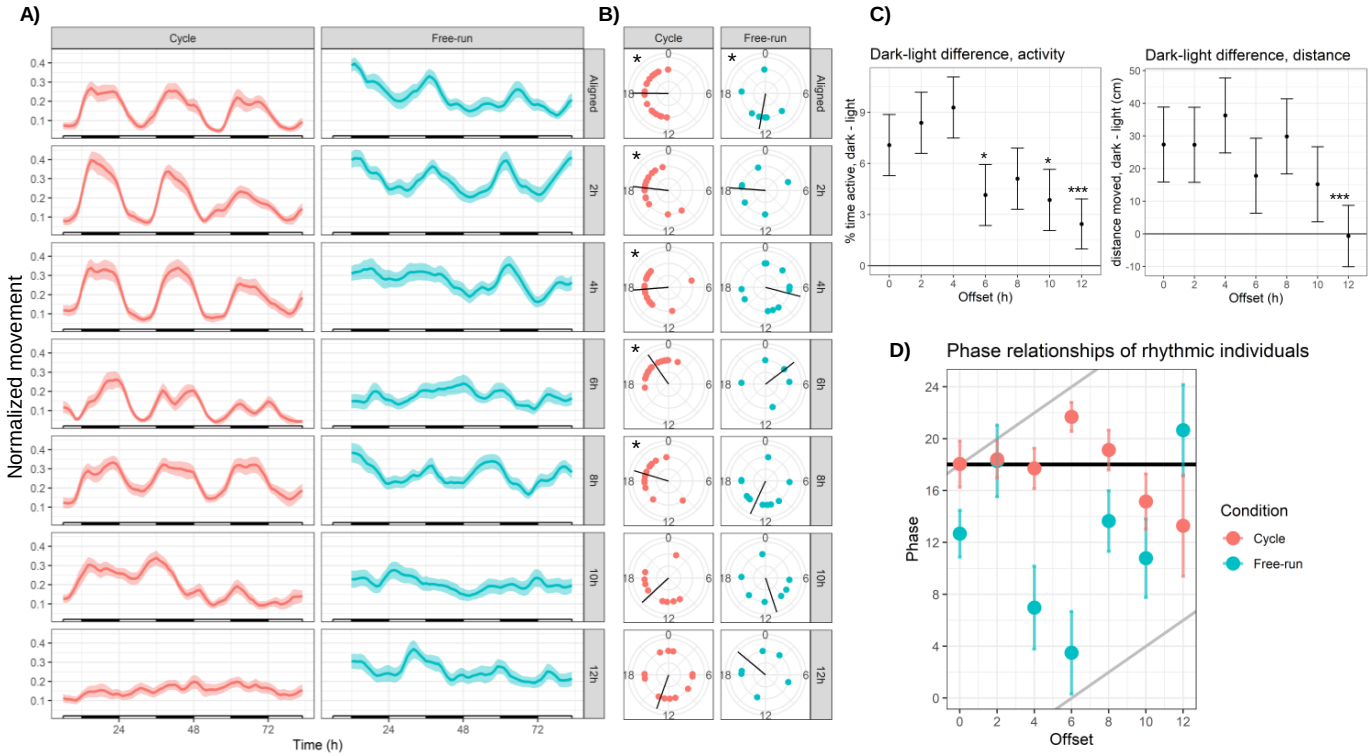

Figure 3. Sensory conflict disrupts circadian locomotor behavior in *Nematostella*. **A)** Mean behavior profiles. Individual locomotor profiles were normalized, averaged, and smoothed (see Methods). Shaded area represents standard error. Left, cycling conditions; white and black bars indicate lights-on and lights-off. Right, free-running at 20 °C and constant darkness; gray and black bars indicate subjective day and night. n=24 for each group except Off12-cycle, where n=36. **B)** Phases of rhythmic animals calculated by MFourFit. Black line represents circular mean. *:Rayleigh test, p<0.05. **C)** Difference, in percentage points, between percent time active per hour during dark and light phases (left), and difference between average distance moved per hour during dark and light phases (right). Asterisks indicate significant difference from Aligned-cycle. *: $p < 0.05$; ***: $p < 0.001$. **D)** Means and standard errors of the phases of rhythmic individuals in each group. Black and grey lines represent expected phases of light-entrained and temperature-entrained rhythms, respectively (see "Relative strengths of light and temperature zeitgebers").

ratio was reduced (LMM, p=0.024). We confirmed that *Nematostella* exhibited "normal" diel behavior under a broad range of light and temperature relationships using clustering analysis. We quantified distances between the 14 mean time series based on their spectral properties using wavelet transformation followed by principal component analysis and hierarchical clustering (see Methods). The Aligned-cycle, Off2-cycle, Off4-cycle, Off6-cycle, and Off8-cycle time series formed a single cluster with high support based on the approximately unbiased (AU) test, apparently corresponding to normal rhythmic behavior, whereas both Off10-cycle and Off12-cycle fell into different clusters (Fig. 4). *Nematostella*'s diel behavior was therefore robust up to an 8h misalignment between light and temperature cycles, although there was a detectable phase delay specifically in the Off6-cycle group.

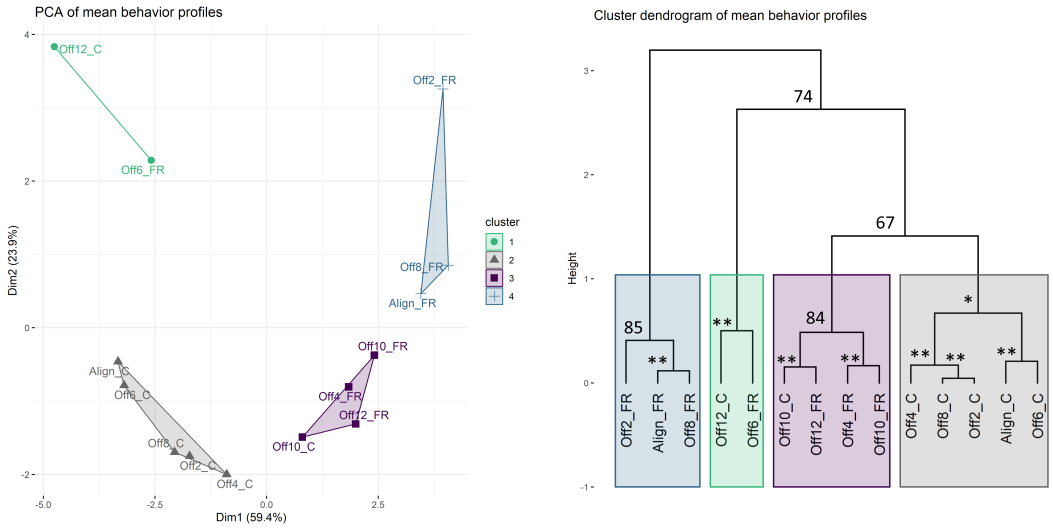

Figure 4. Clustering analysis of mean behavior profiles based on wavelet transformation. A) Principal components analysis of wavelet transformation distance matrix. Time series were grouped and colored based on the clusters identified in B). C: cycles; FR: free-running. B) Hierarchical clustering of samples in principal components space. Colored rectangles indicate the four clusters discussed in the text. Numbers indicate unbiased (AU) P values. *unbiased (AU) P value >= 90; **unbiased (AU) P value >=95.

Sensory conflict disrupts behavior during free-run

Free-running rhythms were disrupted under large degrees of sensory conflict (Off10-FR and Off12-FR), as well as during Off6-FR (Tables 1 and 2, Fig. 3a). The mean behavior of animals in Off6-FR and Off10-FR was totally arrhythmic (LSP and eJTK $p > 0.1$). However, Off8-FR was clearly rhythmic and no weaker than Aligned-FR, demonstrating that the effects of SC on free-running rhythms are not linear. Mean behavior in Off12-FR was rhythmic (eJTK, p=7e-5)—albeit visually disrupted—but the power and amplitude of the mean time series were lower, there were fewer rhythmic individuals, and the variance of the phases of rhythmic individuals was larger compared to Aligned-FR (Table 2). Oddly, Off12-FR was more strongly rhythmic than Off12-cycle; although just 6/24 individuals (25%) were rhythmic, the power of the mean time series was larger than Off12-cycle (Table 2). Thus, antiphasic light and temperature cycles weakened, but did not abolish, endogenous circadian rhythms; instead, free-running behavior was most strongly disrupted at intermediate (6h and 10h) offsets. In the clustering analysis, Aligned-FR, Off2-FR, and Off8-FR formed one cluster with moderate AU support, while Off4-FR, Off10-FR, and Off12-FR formed a third cluster that also included Off10-cycle, again with moderate AU support (Fig. 4). The fourth

cluster was strongly supported and consisted of Off6-FR and Off12-cycle, two groups with severely disrupted rhythms.

There were no significant differences between the mean powers of behavioral rhythms across free-running groups (Dunn test, $p>0.05$), nor was there a clear trend in the number of individuals with significant 24h rhythms (Table 2). Therefore, the weak (or abolished) mean rhythms observed in Off6-FR, Off10-FR, and Off12-FR were largely due to a lack of synchronization between rhythmic individuals. To illustrate this, we re-calculated mean time series restricted only to individuals with significant 24h free-running rhythms. For most groups, including Aligned-FR, this increased the power of the mean time series, indicating that rhythmic individuals were in phase with one another. However, for Off6-FR and Off12-FR, the new mean time series actually had slightly lower power than when using all individuals, indicating total desynchronization among rhythmic animals (Table B in S1 Appendix.). The power of Off10-FR did increase, but was very low to begin with (Table 2). We conclude that the disruption of circadian free-running behavior in Off6-FR and Off12-FR appears to be due primarily to a lack of synchronization among individual animals, and it is notable that some individuals in every experimental group were able to maintain 24h rhythms.

The relationship between light and temperature cycles affected the phase of free-running rhythms, but not according to an obvious pattern. The phase of Off2-FR was advanced by 1.8h relative to Aligned-FR, Off8-FR was advanced by 4.4h, and Off12-FR was advanced by 4.3h (CircaCompare, $p<7\times10^{-3}$). Period length was not affected by sensory conflict (Fig. A in S1 Appendix.).

Relative strengths of light and temperature zeitgebers

To gain insight into the relative strengths of the two zeitgebers, we plotted the means and standard errors of the phases of rhythmic individuals against the offset between light and temperature (Fig. 3d). Rhythms entrained solely by light peak at roughly ZT18 [37, 38], and this is plotted as the black line in Fig. 3d. Temperature-driven rhythms also peak at ZT18 (Fig. 2a), and this is plotted as the grey lines in Fig. 3d. If the phase of a rhythm were determined entirely by light, it would be close to the black line; if determined by temperature, it would be close to the grey lines. We found that phases in the Off4-cycle and Off8-cycle groups were significantly closer to the light (black) line (paired Wilcoxon rank tests, $p<0.05$). The phase distributions of all other groups were approximately equidistant between light and temperature, including every free-running group.

This analysis demonstrates that light and temperature interact to set the phase of circadian behavior in *Nematostella*, but that light exerts strong direct control on behavior. When light and

temperature cycles were close in phase (Aligned and Off2), they acted synergistically the set the phase of locomotor rhythms, while at larger offsets phases were either determined primarily by the light cycle, or were intermediate between light and temperature. We found no evidence that the phases of free-running rhythms were primarily determined by either zeitgeber, with the caveat that this test had less power for free-running groups due to the numbers of rhythmic animals. Although light has strong direct effects on behavior, it is not necessarily a stronger zeitgeber than temperature in terms of setting the phase of free-running rhythms.

Sensory conflict alters transcriptome-wide patterns of rhythmic gene expression

We used 3' tag-based RNA sequencing (Tag-seq) to characterize the effects of sensory conflict on gene expression. Anemones were sampled at 13 time points across 48 h, either under Aligned-cycle or Off12-cycle conditions (Fig. 1c). We refer to Off12-cycle as "SC" for sensory conflict. Reads were mapped to the SimRbase genome (Nvec200_v1, `https://genomes.stowers.org/starletseaanemone`).

The existence of gene expression differences between day and night is a fundamental consequence of circadian rhythms. Under Aligned conditions, 1009 genes (6.6% of the transcriptome) were differentially expressed (DE) between light and dark samples ($p<0.05$), while 627 genes were DE between light and dark during SC, and 277 genes were DE in both time series. The correlation of log-fold changes (LFC) of the 277 shared genes was strongly negative (Pearson's $r=-0.59$), meaning that genes upregulated in the light under Aligned conditions were generally downregulated under SC, and vice versa. Consequently, only 25 genes were DE between light and dark samples when averaged across both time series, and 1747 genes differed in their response to light across conditions (significant Condition:Light interaction). We further quantified the effects of SC on diel gene expression using discriminant analysis of principal components (DAPC), which identifies the linear combinations of variables ("discriminants") that maximize the variance between pre-defined groups [51]. We used DAPC to discriminate between light and dark samples from the Aligned time series; the discriminant axis therefore represents genes with the most variance between light and dark. We then applied the same discriminant function to the SC samples, revealing substantial differences between the transcriptomic profiles of light and dark animals in Aligned and SC conditions (Fig. 5a). Genes that distinguished light and dark samples under Aligned conditions failed to do so under SC, as the density plots of light and dark SC animals substantially overlapped. In fact, the light SC animals

were closer to the dark Aligned animals on the discriminant axis, meaning that the diel expression patterns of many genes were reversed under SC. This demonstrates that SC substantially altered, and in many cases inverted, diel gene expression patterns in *Nematostella*.

Light appears to drive the expression of only a handful of genes, although these 25 genes notably include three putative circadian transcription factors (two PAR-bZIPs and *Helt*). In contrast to light, 1978 genes (13%) had a significant linear response to temperature across all samples. Temperature-responsive genes were enriched for gene ontology (GO) terms related to transcription factor binding and oxidoreductase activity; genes with a significant Condition:Light interaction were also enriched for terms related to transcription factor activity, in addition to nucleoside-triphosphatase activity. This suggests that the temperature cycle has widespread effects on transcription during light-dark cycles by modulating the activity of transcription factors. The mean expression level of 90 genes significantly differed between the Aligned and SC time series. These genes were not enriched for any GO terms, but included one of the aforementioned PAR-bZIP proteins and a cytochrome P450 oxidase (CYP) previously implicated in circadian rhythms in *Nematostella* [38], along with two other CYPs and a SOX-family transcription factor. A large number of genes (1898) displayed a linear change in expression with time, which can be attributed to the fact that animals were not fed during the experiment. Consistent with this, genes with decreasing expression over time were enriched for many GO terms related to metabolism, including "cellular biosynthetic process", "cellular catabolic process", "small molecule metabolic process", "fatty acid metabolic process", "carbohydrate metabolic process", and "cytochrome-c oxidase activity". This suggests an overall downregulation of metabolic processes as the animals went without food over 48h.

We searched 1kb upstream of transcription start sites ("promoters") for putative binding motifs that may play a role in regulating circadian gene expression using the HOMER motif discovery tool. Genes whose mean expression during SC differed from mean expression during Aligned conditions were enriched for a novel motif of unknown function, which was most similar to Myb-related binding motifs in plants (HOMER, $p=1 \times 10^{-12}$; S4 Table), while genes with a negative Condition:Light interaction (i.e. genes with relatively more dark expression during SC) were strongly enriched for numerous bZIP transcription factor binding motifs (HOMER, $p=1 \times 10^{-14}$). Genes whose expression was negatively associated with temperature, and genes whose expression was positively associated with time, were also enriched for bZIP motifs (S4 Table).

In summary, very few genes were differentially expressed in response to light across antiphasic temperature cycles, whereas 13% of the transcriptome showed a linear response to temperature

regardless of light. Some genes had different mean expression levels due to sensory conflict, but the log-fold change was less than 1 in all cases. The set of light-responsive genes, although small, includes the putative circadian transcription factors *Clock*, *Helt*, *PAR-bZIP-a*, and *PAR-bZIP-c*. For complete lists of DE genes and GO enrichment results, see S3 Table.

Rhythmicity analysis

We tested for rhythmic gene expression using RAIN (rhythmicity analysis incorporating non-parametric methods) v1.24.0 [52], a non-parametric approach particularly suited for the detection of asymmetric waveforms. We compared these results to two other pieces of software: ECHO (extended circadian harmonic oscillator, https://github.com/delosh653/ECHO, [53]), a parametric method based on the harmonic oscillator equation, and DryR (https://github.com/naef-lab/dryR, [54]), another parametric approach based on harmonic regression and incorporating Bayesian model selection. Encouragingly, there was strong agreement between the three programs despite their completely different statistical methodologies. 90% of rhythmic genes identified by RAIN ($p<0.01$) had an adjusted ECHO p-value less than 0.05, and 94% of genes with an ECHO p-value less than 0.01 had a RAIN p-value less than 0.05. Log p-values of ECHO and RAIN were highly correlated ($r = 0.85$). DryR does not calculate p-values, but instead uses model selection to cluster genes based on their expression profile. Briefly, 81% of genes assigned rhythmicity in either time series by DryR were rhythmic in that time series based on RAIN ($p<0.01$), and 93% had a RAIN p-value less than 0.05; 73% of rhythmic RAIN genes ($p<0.01$) were assigned to the corresponding cluster(s) in DryR. Thus RAIN and DryR also showed good agreement, although RAIN tended to identify additional rhythmic genes not clustered by DryR. We focus on the output from RAIN, and the output of the other two programs is available in S2 Table.

Under Aligned conditions, 2868 genes displayed 24h rhythms in expression (RAIN, $p<0.01$; 18% of the transcriptome). During sensory conflict, 2440 genes were rhythmic ($p<0.01$; 16%), and 1116 genes were rhythmic in both time series (Fig. 5a). Thus, there were similar overall numbers of rhythmic genes in the two conditions, but less than half of them were shared. To define sets of condition-specific rhythmic genes, we excluded genes that were marginally significant in the other condition ($p<0.1$); by this metric, 1225 genes lost rhythmicity during SC (Align-specific) and 921 gained rhythmicity (SC-specific). The gain and loss of rhythmicity for large numbers of genes was thus not simply an artifact of strict p-value cutoffs, and was also confirmed by the DryR analysis (S2 Table). The promoters of genes that were rhythmic in both Aligned and SC time series were enriched

for bZIP transcription factor binding sites ($p=1 \times 10^{-6}$), while the promoters of Aligned-specific and SC-specific rhythmic genes were not enriched for any motifs (S4 Table).

Genes with rhythmic expression under Aligned conditions were enriched for various GO terms related to metabolism, and several KEGG terms related to RNA and protein metabolism (Table 3). Align-specific genes (genes that lost rhythmicity under SC) were enriched for several of these metabolic GO terms, as well as the KEGG term "Ribosome". Genes that were rhythmic during SC were enriched for 5/16 of the terms enirched during Aligned conditions, in addition to GO terms related to DNA binding, and the KEGG terms "Autophagy" and "ABC transporters" (Table 4). SC-specific genes were not enriched for any GO or KEGG terms. Overall, many genes with rhythmic expression performed metabolic functions, including RNA and protein metabolism, and many of these rhythmic metabolic genes lost rhythmicity under SC. For full GO and KEGG enrichment results, see S3 Table.

Table 3. Functional enrichment of Aligned rhythmic genes

Term	P-value	Type
macromolecule biosynthetic process	0.0011	BP
cellular nitrogen compound biosynthetic process*	0.0015	BP
biosynthetic process*	0.0015	BP
cellular amide metabolic process*	0.0047	BP
regulation of metabolic process	0.029	BP
organonitrogen compound biosynthetic process*	0.034	BP
structural molecule activity*	0.0047	MF
GTPase activity	0.0056	MF
hydrolase activity, acting on acid anhydrides	0.034	MF
Ribosome*	2.2×10^{-9}	KEGG
Phagosome	0.0036	KEGG
Spliceosome	0.0037	KEGG
Mitophagy - animal	0.0050	KEGG
Endocytosis	0.026	KEGG
Protein processing in endoplasmic reticulum	0.027	KEGG
RNA transport	0.045	KEGG

*: Term also enriched in Align-specific genes.

The phases of Aligned rhythmic genes were not uniformly distributed around the clock (Rayleigh test of uniformity, $p=1 \times 10^{-4}$). Instead, there were two peaks in the phase distribution roughly 10h apart, one at mid-morning (ZT4) and one in early night (ZT14); 24% of rhythmic transcripts peaked between ZT2-6, and 28% peaked between ZT12-ZT16 (Fig. 5c). The phase distribution under SC was also bimodal, with peaks in the mid-morning and early night (Fig. 5c), although the two distributions were not identical (Rao's two-sample test for circular homogeneity, p=0.046). Despite this similarity, the placement of genes within those distributions was very different. Of the

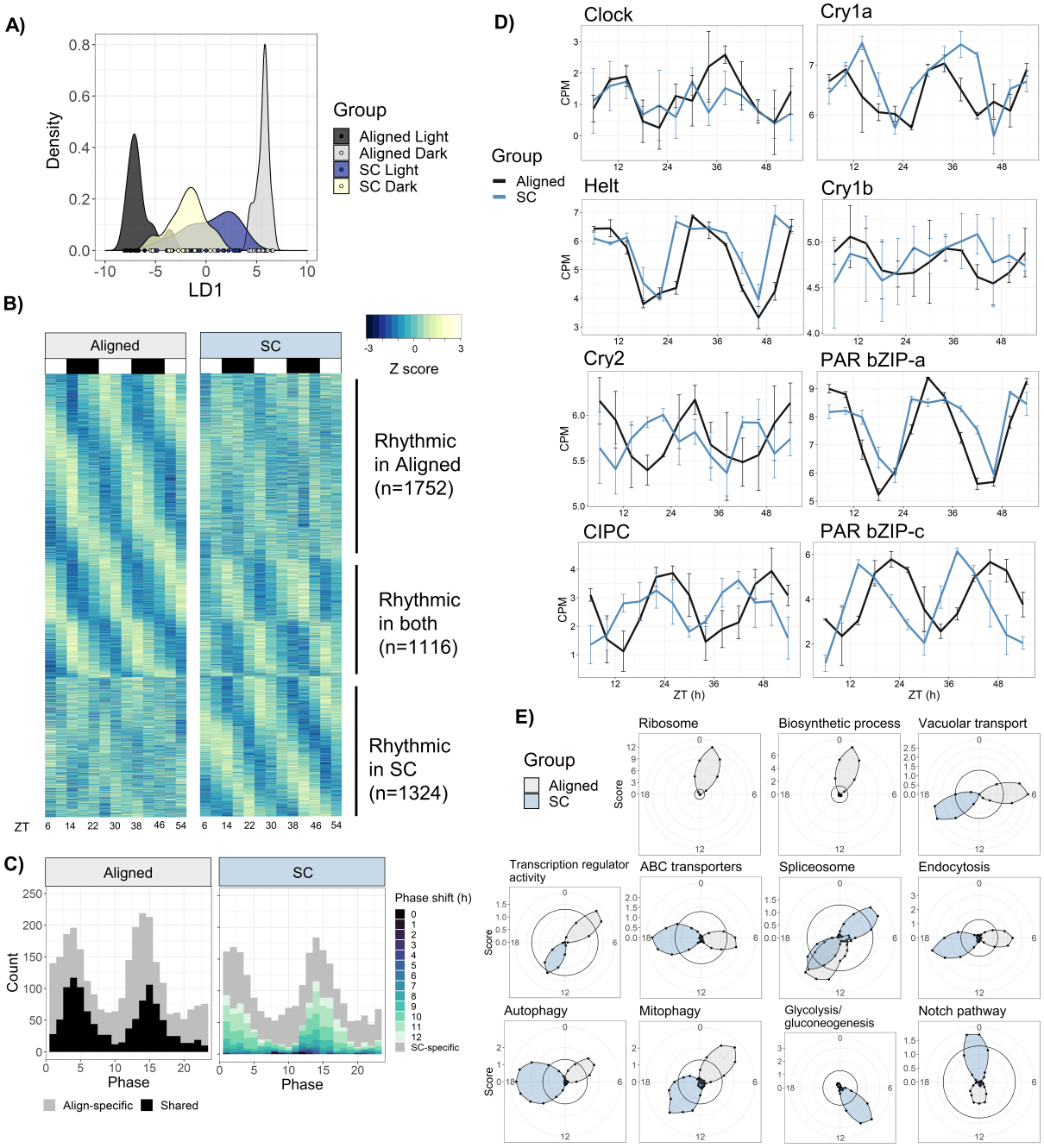

Figure 5. Sensory conflict alters transcriptome-wide patterns of rhythmic gene expression. A) Discriminant analysis of principal components (DAPC) demonstrates shifts in diel gene expression under SC. Density plot of sample loading values of light and dark samples during aligned and conflicting zeitgeber cycles, on 1st discriminant axis from DAPC of aligned samples ("LD1"). **B)** Heatmaps of normalized rhythmic gene expression. Replicates were averaged at each time point and Z-scores were calculated for each gene and time series. Genes were considered "rhythmic" if they received a RAIN p-value < 0.01 in the Aligned time series (top), SC time series (bottom), or both (middle). White and black rectangles represent light and dark time points, respectively. **C)** Phase distributions of rhythmic genes in Aligned (left) and SC (right) time series. Grey genes were rhythmic in only one time series, and black and colored genes were rhythmic in both. In SC, the color of shared rhythmic genes represents the phase shift of that gene from the Aligned time series. **D)** Phases of core clock genes under Aligned and SC conditions. Lines show mean counts per million, and error bars represent 95% confidence intervals. **E)** Sliding window enrichment analysis of select GO and KEGG terms during Aligned and SC time series. P-values were calculated by comparing genes with peak phase within a 4h sliding window with all other genes, and the score (y-axis) at each point is the average adjusted -log10 p-value at that time point (see Methods). Black circles indicates an FDR threshold of 0.05.

Table 4. Functional enrichment of SC rhythmic genes

Term	P-value	Type
regulation of metabolic process	0.00083	BP
DNA binding	0.038	MF
hydrolase activity, acting on acid anhydrides	0.044	MF
protein dimerization activity	0.044	MF
sequence-specific DNA binding	0.044	MF
Mitophagy - animal	0.0001	KEGG
Spliceosome	0.0003	KEGG
Autophagy - animal	0.0022	KEGG
ABC transporters	0.028	KEGG
Endocytosis	0.028	KEGG

1116 genes that were rhythmic under both Aligned and SC conditions, the vast majority (1092/1116, 98%) shifted in phase relative to the light cycle, with a median (absolute) phase shift of 10.3h (CircaCompare, $p<0.01$); 86% shifted by at least 6h, and 58% by 10-12 h. Only 24 genes did not shift in phase relative to the light cycle—notably, this includes *Clock* itself, as well as *Helt* and one of the PAR-bZIPs (8136) (Fig. 5b); this list of genes overlaps with, but is not identical to, the 25 genes DE with respect to light. We found that just 10% (113 / 1116) of genes that were rhythmic in both conditions shifted in phase relative to the temperature cycle (CircaCompare, $p<0.01$). We identified 647 genes that shifted in phase by 10-12h relative to the light cycle and did not shift in phase relative to the temperature cycle; these genes closely tracked the phase of the temperature cycle and may be directly regulated by temperature. They were enriched for GO terms related to transcription factor activity, and the KEGG terms "Mitophagy" and "Spliceosome" (S3 Table).

Since the function of circadian clocks is to orchestrate the coordinated expression of biological processes on diel scales, we performed functional enrichment of rhythmic genes that peaked at particular times of day using a sliding window approach (see Methods). This analysis revealed dramatic changes to the expression of functionally-related genes, particularly genes that mediate metabolic processes, during SC (Fig. 5e). Only a single GO or KEGG term, "Spliceosome", was enriched at the same time of day for both time series. Most terms that were enriched among aligned rhythmic genes were not enriched at any time during SC. Under aligned conditions, GO and KEGG terms related to macromolecule and protein metabolism were enriched in early morning (ZT0-3) and lost enrichment under SC; "RNA transport" and "ubiquitin-mediated proteolysis" were enriched in early night (ZT13-14) and lost rhythmicity under SC. Terms whose expression shifted from day to night during SC included "transcription factor activity", "vacuolar transport", "hydrolase activity", "autophagy", "mitophagy", "ABC transporters", and "mRNA surveillance pathway"; "protein processing in ER" shifted from ZT10 to ZT4 (S3 Table). Some terms were only enriched

under SC: "DNA binding" and "Notch signalling pathway" in the early day, "helicase activity", "ATP binding", and "GTPase activity" in mid-night, and several KEGG terms related to carbon metabolism during the late day, including "Glycolysis" and "Pyruvate metabolism" (S3 Table).

During SC, the amplitudes of shared rhythmic genes (n=1116) were reduced by a median of 7.1% (Wilcoxon, $p=2 \times 10^{-4}$; Figure D in S1 Appendix). This was primarily driven by a reduction in amplitude of genes that followed the phase of the temperature cycle (n=647, see section "Rhythmicity analysis"). These temperature-responsive genes had much higher amplitudes than other shared genes across both time series (+16.4%), but during SC their amplitude was reduced by a median of 8.8% (Wilcoxon, $p=7 \times 10^{-4}$). The amplitudes of Align-specific and SC-specific genes did not differ from each other (Wilcoxon, p=0.49), and were collectively 15% lower than the amplitudes of shared rhythmic genes (Wilcoxon, $p=2 \times 10^{-16}$). Mean expression of shared rhythmic genes did not differ during SC (p=0.9), but the expression of SC-specific genes was 18% lower than that of Align-specific genes, during their respective time series (Wilcoxon, $p=1 \times 10^{-8}$; Figure D in S1 Appendix). The net result was that the median expression level of rhythmic genes was 7.9% lower during SC. These results suggests that there is a core set of genes that are robustly rhythmic under contrasting light and temperature regimes, and follow the phase of the temperature cycle. However, these genes oscillated more strongly when light and temperature cycles were aligned.

An estuarine organism like *Nematostella* could be influenced by circatidal rhythms, although circatidal behavior rhythms are not consistently observed [37, 39]. We identified 268 genes with significant 12h periods in aligned conditions and 440 in SC (RAIN, p<0.01), with 8 genes shared between the two conditions (S1 Appendix; S2 Table). These genes were not enriched for any GO terms. Although our sampling design (every 4h) is not well-suited to detect circatidal rhythms, it seems that circatidal gene expression is less prominent than circadian gene expression in *Nematostella*, in agreement with previous work [39].

Comparison with light cycles at constant temperature

In order to assess how rhythmic gene expression during simultaneous light and temperature cycles compares to gene expression during a light cycle at constant temperature, we re-analyzed a previous study, Oren et al. (2015), that sampled *Nematostella* during an LD cycle at constant temperature (23°C) [38]. We re-analyzed their raw data using the same software and methods as in the current study, including mapping to the SimrBase genome. The phases of clock genes between [38] and the current study are shown in Table 5, and this comparison is discussed in more detail in S1 Appendix.

Briefly, core circadian genes (*Clock*, *Helt*, *CIPC*, cryptochromes, and PAR-bZIPs) had similar phases in our Aligned time series and in Oren et al. (within 4h, the resolution of time points in both studies), with the exception of *Cry1b*. There was little overlap between rhythmic genes overall: only 477 / 1498 (32%) genes rhythmic in Oren et al. (RAIN, $p<0.05$) had a p-value less than 0.05 in the current study, and just 224 (47%) of these had phases within 4h of each other. Consequently, functional enrichment of Oren et al. (2015) was also dissimilar to the current study (S3 Table)—only a single KEGG term, "Spliceosome", was enriched at the same time of day (ZT12-18). These differences could certainly be due to the temperature cycle. However, Oren et al. used *Nematostella* derived from a different population than the current study (Maryland versus Massachusetts), and differences in other factors, such as diet and time of feeding, could also affect the rhythmic transcriptome. Regardless of differences in clock output, which can be variable between tissues, conditions, and populations, our re-analysis shows that core clock gene expression was not altered by the addition of a temperature cycle in-phase with the light cycle.

Table 5. Comparison of phases of putative clock genes

Study	Clock	Helt	CIPC	PAR-bZIP-a	PAR-bZIP-c	Cry1a	Cry1b	Cry2
Current study (Aligned)	12.4	9.2	1.0	7.3	22.3	9.3	10.5	5.6
Current study (SC)	11.94	7.9	19.3	8.0	16.2	12.1	NA	21.8
Oren et al. (2015)*	10.9	7.3	23.4	5.3	19.4	7.9	NA	2.3
SimrBase ID	6258	15017	4651	8136	8448	8109	8041	15282
JGI ID	160110	246249	245026	150375/ 87565	39846	168581	106062	194898

Phases estimated with CircaCompare. NA: below significance cutoff, phase not calculated. We used a p-value cutoff of p=0.01 for the current study, and p=0.05 for [38] because of their small sample size.

Network analysis

We used weighted gene co-expression network analysis (WGCNA) to identify gene modules with similar temporal expression. First, we assessed how SC affected network topology and module identity by comparing Align-specific and SC-specific networks constructed separately for genes

rhythmic in each time series. Although we found that few GO and KEGG terms were shared between modules in the two networks, we also identified some gene modules that were more robust to SC than others, and the co-expression patterns of rhythmic genes were surprisingly well-preserved in the SC network. Second, we constructed a Full network using all genes rhythmic in either time series. In addition to identifying additional groups of co-expressed rhythmic genes, this approach also revealed that rhythmic gene expression was less well-correlated both within and across modules during sensory conflict. The timing of module expression in the Full network is shown in Fig. 6b, the expression of select modules is shown in Fig. 6a, and the relationships between modules in all three networks in shown in Fig. 6c. The expression of all modules in all networks is shown in S1 Appendix, and functional enrichment results are available in S3 Table. In the following section, modules are referred to with color names, followed by an abbreviation indicating which network they belong to. For example, the Blue module in the SC-specific network is Blue-SC, whereas the Blue module in the Full network in Blue-F.

Genes in the Align-specific network (2868 genes, 39 samples) were assigned to 6 modules, with 889 genes (31%) unassigned. All module eigengenes—the first principal component of the module expression matrix—were rhythmic (LSP, $p<0.01$). Modules with daytime peak expression were enriched for processes related to translation, ribosomes, and nitrogen compound biosynthesis (Blue-A); and transcription factor activity, vacuolar transport, and GTPase activity (Turquoise-A). A module with peak expression at ZT12 was enriched for catabolic processes, including proteolysis and RNA degradation (Yellow-A). Modules with night-time peak expression were enriched for ATP binding, chaperone activity, chromatin organization, and the spliceosome (Brown-A); and "negative regulation of cellular macromolecule biosynthetic process" (Green-A). Genes in the SC-specific network (2440 genes, 39 samples) were assigned to 9 modules, with 1080 genes (44%) unassigned. Modules with peak daytime expression were enriched for a single GO term, "ion channel complex" (Black-SC); and the KEGG terms "Spliceosome" and "protein processing in the ER" (Blue-SC). A module with peak expression in the late day was enriched for "protein folding" and several KEGG terms related to carbon and amino acid metabolism, including glycolysis (Brown-SC). Modules with peak night-time expression were enriched for proteolysis and peptidase activity (Pink-SC); terms related to DNA repair (Red-SC); and transcription factor activity, endocytosis, mitophagy, and autophagy (Turquoise-SC).

Cross-tabulating genes in each module across the two networks revealed that the majority of genes in most modules were either arrhythmic or unassigned in the other network (Figure C in S1

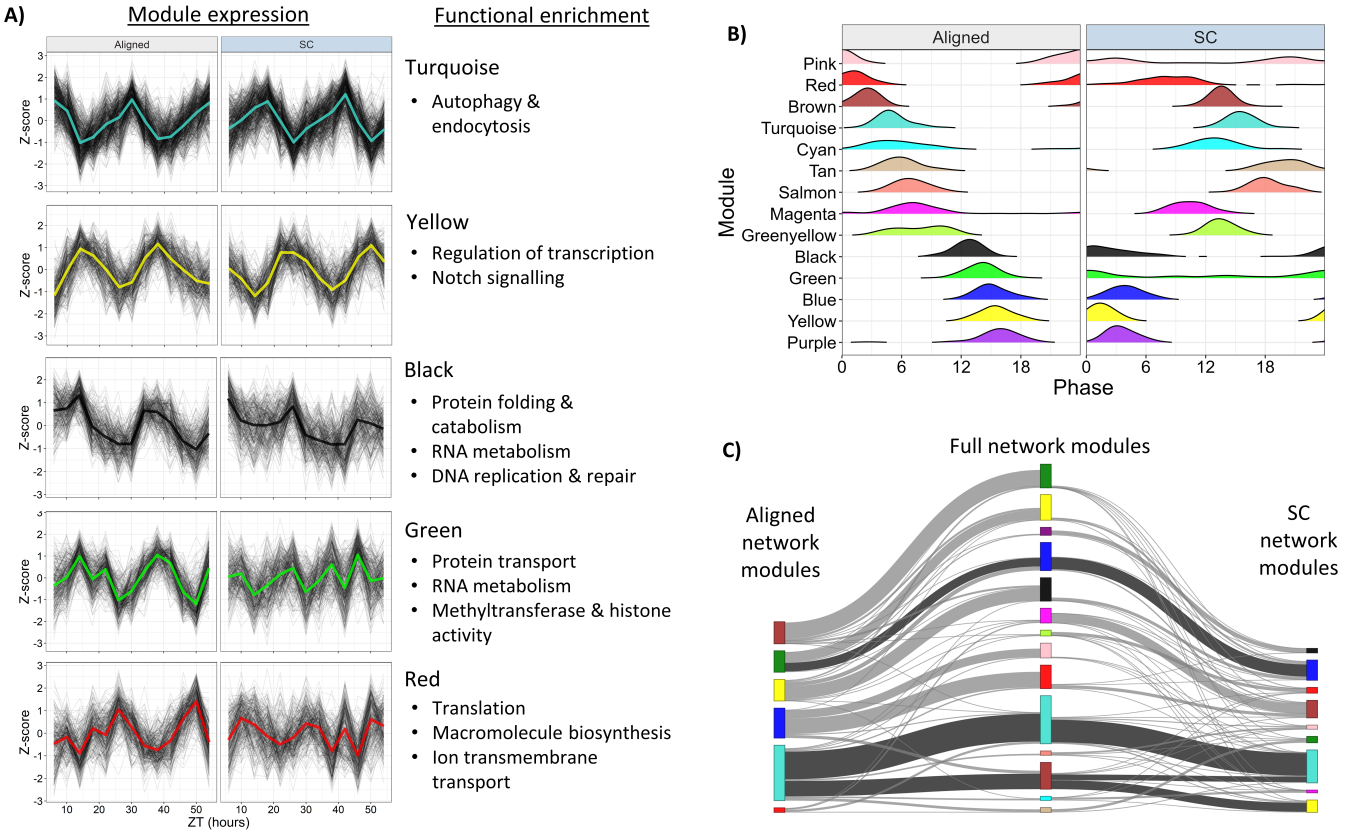

Figure 6. Network analysis identifies changes to rhythmically co-expressed gene modules. **A)** Expression patterns of select modules in the full network. Black lines are Z-scores (difference from mean divided by standard deviation) of the expression of each gene, and the colored line is the mean of those Z-scores. Left panels are Aligned samples, and right panels are SC samples. Functional enrichment **B)** Phase distributions of modules genes in the Full network during Aligned (left) and SC (right) conditions. Each line shows a smoothed density estimate of the phases of rhythmic genes within that module, weighted by the -log10(p-value) from RAIN. **C)** Sankey plot showing gene overlap between modules in the Align-specific (left), Full (middle), and SC-specific (right) networks. Height of module bars represents the number of genes in that module, and the width of connections represents the number of shared genes. Dark connecting lines indicate highly significant ($p<1 \times 10^{-5}$) overlap between Aligned and SC network modules. Genes in grey modules are not shown. Color labels were assigned independently for each network (no inherent meaning).

Appendix). However, two modules in the Aligned network (Turquoise-A and Green-A) had strong overlap with modules in the SC network (hypergeometric test, $p<<1 \times 10^{-5}$) and two other modules had moderate overlap (Yellow-A and Red-A, $p=1 \times 10^{-4}$ and $p=4 \times 10^{-3}$). The Blue-SC module had significant overlap with the Green-A module ($p=6 \times 10^{-28}$) and the Yellow-A module ($p=9 \times 10^{-4}$), but these modules did not share any GO or KEGG terms. The Turquoise-SC module overlapped with the Turquoise-A module ($p=1 \times 10^{-50}$) and the Red-A module ($p=0.02$); Turquoise-A and Turquoise-SC shared the GO terms "vacuolar transport", "DNA-binding transcription factor activity", and "GTPase activity", and the KEGG terms "Endocytosis", "Mitophagy", and "Autophagy." Finally, the Yellow-SC module also overlapped with the Turquoise-A module ($p=6 \times 10^{-30}$), and shared

the GO terms "regulation of transcription, DNA-templated," "DNA-binding transcription factor activity", and "sequence-specific DNA binding." From this analysis, we can see that genes that perform certain functions, including endocytosis and transcription factor activity, maintained temporally-coordinated expression during SC and shifted in phase "together". However, just 25% of GO and KEGG terms enriched among Aligned network modules were enriched in any SC network module, which illustrates that SC substantially disrupted the rhythmic expression of many functionally-related groups of genes.

We compared module preservation across the two networks in more detail using statistics that quantify the preservation of underlying network properties (as opposed to cross-tabulation, which only considers module assignments). Comparing the aligned and SC networks, we considered density-based statistics—which test whether genes in a module remain densely connected to one other in both networks—and connectivity-based statistics–which test whether the correlation patterns between genes remain similar (see [55] for details). Significance was assessed with permutation tests and summarized with Z-statistics (Z-density, Z-connectivity, and the average of the two, Z-summary), with a Z-statistic of >10 indicating strong evidence of module preservation [55]. We also calculated these statistics for a random sub-sample of genes from the Aligned network, the "Gold" module. Using this approach, 5/6 modules in the Aligned network had strong evidence for preservation in the SC network (Z-summary>10), and the sixth module (Red-A) had moderate evidence for preservation (Z-summary=9.7; Table 6). Even the randomly sampled "Gold" module was strongly preserved by this metric. However, there were differences between the density- and connectivity-based statistics. Z-connectivity was actually highest in the Gold module, which represents the entire Aligned network. This means that the preservation of connectivity between genes was a property of the entire network and not of particular modules. This counter-intuitive result makes sense if we consider that one of the major effects of SC was a phase shift of 12h. If two genes shift in phase by similar amounts, their pairwise connectivity will be preserved, regardless of whether their connectivity was high or low to begin with. Therefore, we suggest that connectivity was largely preserved between the two networks because many genes shifted in phase by similar amounts. On the other hand, every module had higher Z-density than the Gold module, meaning that genes in a particular module tended to remain more densely connected in the SC-specific network than random pairs of rhythmic genes. This suggests that Z-density is a more appropriate measure of module preservation than Z-connectivity in this case. By this metric, Turquoise-A was the best-preserved module—which matches the cross-tabulation results (Fig. C in S1 Appendix)—followed by Brown-A, Blue-A, Green-A, Yellow-A,

and finally Red-A (Table 6). To summarize, genes that were well-connected in the Aligned network remained generally well-connected during SC, genes that were not well-connected remained poorly connected, and genes co-expressed in the same module remained more densely connected than random pairs of genes.

Table 6. Preservation statistics of modules identified in the Aligned network, assessed in the SC network

Module	Z-summary	Z-density	Z-connectivity
Gold	22.3	13.4	31.1
Grey	9.8	4.9	14.8
Blue	24.2	29.0	19.4
Brown	26.5	33.0	20.1
Green	18.9	27.8	10.1
Red	9.7	13.8	5.6
Turquoise	34.4	49.8	19.0
Yellow	16.8	22.7	11.0

The "Gold" module is a random sub-sample of 1000 genes from the Aligned network; the "Grey" module is rhythmic genes that were not assigned to any module in the Aligned network.

The high preservation of connectivity and density patterns between rhythmic genes during SC may seem surprising given that the overlap between modules in the two networks was limited (Fig. 6c; Fig. C in S1 Appendix). However, these statistics only test whether preservation is higher than would be expected between random pairs of genes chosen from the SC network; we show below that connectivity pattern were in fact weakened during SC. Rhythmicity can also be disrupted even if connectivity is preserved. For instance, the Blue-A and Brown-A module eigengenes lost rhythmicity in the SC samples (Figure E in S1 Appendix; LSP $p>0.1$), meaning that the rhythmicity of genes in these modules was disrupted by SC, although they remained well-connected to one another.

Connectivity patterns were weakened during SC, even though they were not totally disrupted. In the Full network (4192 genes, 78 samples), rhythmic genes were assigned to 14 modules, with 932 genes (22%) unassigned. The correlation between genes and their respective eigengene (kME) was reduced by a median of 5.6% during SC across all modules (Wilcoxon, $p=6\times10^{-15}$), and intramodular connectivity (kIM), a measure of co-expression with other genes in the same module, was reduced by 23% (Wilcoxon, $p<2\times10^{-16}$). The proportion of each gene's expression variance explained by eigengene expression (propVar) was also lower in SC samples (Wilcoxon, $p=1\times10^{-11}$), with a median reduction of 8.2%. These metrics (kME, kIM, and propVar) were significantly lower during SC whether they were calculated for all genes assigned to a module (n=3260), only for assigned genes rhythmic in their respective time series (n=2417 and n=1893), or only for assigned

genes rhythmic in both time series (n=1050). Broken down by module, 5 modules containing 1702 genes (Turquoise-F, Red-F, Black-F, Green-F, and Pink-F) had lower kME, kIM, and propVar during SC (Wilcoxon, $p<0.05$), while 3 modules containing 648 genes had higher values (Blue-F, Purple-F, Magenta-F); Greenyellow-F (74 genes) had higher kME and kIM, with no difference in propVar. The remaining modules had no significant differences. These metrics are density statistics that describe the "tightness" of gene expression within modules, and would be maximized if all genes in a module were perfectly correlated with one another. Therefore, module density was generally weaker during SC. Some modules did gain tighter expression during SC, but they contained fewer than half as many genes as modules that became less densely-expressed. The connectivity of each gene to all other genes in the Full network (kTotal) was median 12% lower during SC (Wilcoxon, $p<1 \times 10^{-15}$). If calculated separately for the two condition-specific networks, kTotal was 31% lower during SC, and kIM was 43% lower (Wilcoxon, $p<1 \times 10^{-15}$). Together, these results show that rhythmic gene expression was less well-correlated both within and across modules during SC.

Half (7/14) of the module eigengenes were robustly rhythmic in both time series; these modules contained 49% of rhythmic genes, and all shifted in phase by 10-12 hours during SC. In other words, the only modules to maintain strong rhythmicity during SC all closely followed the temperature cycle. Two of these modules were negatively correlated with temperature (linear model, $p<0.05$) and shifted from daytime expression during aligned conditions to night-time expression during SC. The Brown-F module (n=341) was enriched for transcription factor activity, and its promoters were strongly enriched for bZIP binding motifs (HOMER, $p=1 \times 10^{-13}$). The Turquoise-F module (n=614) was enriched for many terms related to autophagy and endocytosis, as well as mRNA surveillance and nucleoside-triphosphatase activity; Turquoise-F promoters were also enriched for bZIP binding motifs (HOMER, $p=1 \times 10^{-8}$). Two other modules shifted from daytime to night-time expression, but were not directly correlated with temperature because they peaked at the mean temperature. The Tan-F module (n=61) was enriched for ATP hydrolysis activity and ABC transporters, and the Salmon-F module (n=55) was enriched for serine-type endopeptidase activity and its promoters were (marginally) enriched for ETS binding motifs (HOMER, $p=1 \times 10^{-5}$). The Black-F (n=298), Blue-F (n=359), and Yellow-F (n=327) modules were positively correlated with temperature and shifted from expression during the early night under Aligned conditions to daytime expression during SC. Black-F was enriched for terms related to protein processing and catabolism, RNA metabolism, chromatin organization, and DNA replication and repair. Blue-F was enriched for "Spliceosome", "protein processing in ER", and "Butanoate metabolism." Yellow-F was enriched for regulation of

transcription, protein dimerization activity, and Notch signalling.

Two module eigengenes lost rhythmicity under SC (LSP, $p<0.01$ for Align and $p>0.05$ for SC), Green-F and Pink-F. The Green-F module (n=302) was enriched for GO terms related to RNA metabolism, protein transport, and regulation of gene expression, and contained the Clock gene. Green-F module promoters were enriched for putative binding motifs with unknown function (HOMER, $p=1 \times 10^{-10}$). The Pink-F module (n=189) was enriched for the KEGG term "Sphingolipid metabolism". The Red-F module (n=299) was marginally rhythmic under SC (LSP, p=0.019), and advanced in phase by 8h (Fig. 6b). This module was enriched for proton transmembrane transport and terms related to translation. Two module eigengenes gained rhythmicity under SC, Purple-F (n=101) and Greenyellow-F. Purple-F was enriched for thiamine and purine metabolism, and its promoters were enriched for helix-turn-helix (HTH) binding motifs (HOMER, $p=1 \times 10^{-5}$). The Cyan-F (n=52) and Magenta-F (n=188) modules were marginally rhythmic in Aligned conditions (HOMER, $p<0.02$), and shifted in phase by 4h and 8h, respectively, during SC. Cyan-F was enriched for the KEGG terms "glycolysis" and "TCA cycle", but this enrichment was driven only by two genes, both of which were annotated as phosphoenolpyruvate carboxykinases (PEPCK) S2 Table. Cyan-F module promoters were enriched for SOX binding motifs (HOMER, $p=1 \times 10^{-10}$). Magenta-F was enriched for terms related to protein catabolism, oxidoreductase activity, and RNA transport.

Discussion

We show here that temperature cycles drive and entrain circadian behavior in the cnidarian *Nematostella vectensis*, and explore how the relationship between simultaneous light and temperature cycles affects rhythmic behavior and gene expression. Circadian behavior was disrupted, although not completely abolished, under large degrees of sensory conflict (SC), such as when light and temperature cycles were in antiphase to one another. This points to limits of the clock's ability to integrate information from conflicting environmental signals, and indicates that neither zeitgeber completely dominates the other. Gene expression rhythms were also dramatically altered by SC. Surprisingly, only a small number of genes directly responded to light, whereas several hundred genes directly followed the temperature cycle, and many other genes lost or gained rhythmicity. The net result of these transcriptomic changes was that the temporal expression of metabolic processes was substantially altered; for instance, genes related to autophagy and endocytosis shifted

in phase following the temperature cycle, while genes related to ribosome and protein metabolism lost rhythmicity. The effects observed here are not acute responses to transient environmental disruptions, but chronic changes measured after weeks of exposure and acclimation to SC.

Temperature cycles

Temperature cycles drive and entrain circadian locomotor behavior in *Nematostella*. Temperature cycles can introduce artifacts due to temperature stress or sudden jumps in temperature, but we avoided these issues by testing two ramped, gradually-changing temperature cycles (8–32 °C and 14–26 °C) within the range of diel variation experienced by the source population of experimental animals [39, 56]. Temperature-entrained free-running rhythms are detectable but apparently not very robust; however, the proportion of free-running individuals was comparable to light-entrained free-running rhythms from a previous study (35% vs. 33%) [39], suggesting that free-running rhythms are simply weak in *Nematostella* in general. Nonetheless, this further supports the near-universal ability of circadian clocks to entrain to environmental temperature cycles.

Effects of simultaneous light and temperature cycles on behavior

Nematostella exhibited robust circadian rhythms in locomotor behavior during aligned light and temperature cycles, and rhythmic behavior remained in phase with the light cycle up to approximately 8h of offset between zeitgebers (Fig. 3a). Given that white light exerts strong direct effects on behavior in *Nematostella*, masking free-running locomotor rhythms [38, 39] and inducing rapid contraction of the body and tentacles (Personal obs.), we wondered whether *Nematostella* would simply synchronize their behavior to the light cycle to the exclusion of temperature. This was not the case. During 10-12h SC, rhythmicity was disrupted and *Nematostella* were specifically more active during lights-on, which is normally a period of reduced activity (Fig. 3c). Overall, light was more important than temperature for setting the phase of locomotor rhythms under most conditions, but there was no clear relationship between either zeitgeber and the phase of free-running rhythms (Fig. 3d). The alteration of free-running behavior during SC demonstrates that temperature cycles and light cycles interact to influence endogenous rhythms.

In *Drosophila*, behavioral rhythms become abnormal and "plateau"-like under intermediate (6h) degrees of SC, which is accompanied by the breakdown of central clock oscillations, but behavioral rhythms and central clock oscillations preferentially synchronize to light under 12h misalignment [4]. On the other hand, *Drosophila* peripheral clock oscillations seem to preferentially entrain to light

under all conditions [22]. In this sense, *Nematostella*'s behavior was more like the *Drosophila* central clock, because behavior was disrupted under some conditions rather than simply following a single zeitgeber.

Rhythmic behavior is the result of direct (e.g. acute responses to light) and indirect (e.g. entrainment of the circadian clock) effects of environmental signals, which can result in non-linear behavioral responses. When light and temperature cycles were offset by 12h, behavioral rhythms during the cycles were actually weaker than free-running rhythms, which indicates a masking effect. More specifically, entrainment to 12h SC weakened, but did not abolish, free-running circadian rhythms, and rhythms were further disrupted by conflicting light and temperature cycles. Conversely, when light and temperature were offset by 6h, free-running rhythms were profoundly disrupted and there was roughly normal rhythmic behavior during the cycles (Fig. 3a). This shows that environmental cycles can drive rhythmic behavior even if the clock itself is disrupted. Although it is intuitive that behavioral rhythms should gradually diminish as SC increases, which was the case for cycling conditions, it is not obvious why free-running rhythms were weaker during 6h and 10h SC than 8h and 12h. Understanding this non-linear behavior will probably require untangling the molecular pathways that connect light and temperature to the clock.

Implications for putative core clock genes

We have little functional information about the molecular architecture of cnidarian clocks. In addition to orthologs of *Clock* and *Cycle*, *Nematostella* possesses several genes that are suspected to have central roles in circadian regulation because of their homology to bilaterian clock genes and their strong rhythmicity across multiple studies [38, 39, 41]. Candidate negative regulators of *Clock* include *Helt*, *CIPC*, *Cry2*, and *PAR-BZIP-c*, while other cryptochromes (*Cry1a* and *Cry1b*) are candidate photosensors, and another PAR-bZIP (*PAR-bZIP-a*) may be an activator of *Clock* [40]. All of these genes, except for *Cry1b*, were strongly rhythmic during both aligned and SC conditions, consistent with their apparent importance in *Nematostella*'s circadian rhythms. Specifically, our data support the hypothesis that *Cry2* is involved in the core clock, because its rhythmic expression can be driven by both light and temperature cycles, while rhythmic expression of *Cry1a* and *Cry1b* appears to be driven only by light cycles. This is consistent with previous observations that *Cry1a* and *Cry1b* expression is strongly induced by blue light [41, 57], although we note that these genes are not homologous to bilaterian Type-I photosensor cryptochromes [47]. In addition, since the phase of *Cry1a* shifted by ∼3h during SC, and *Cry1b* lost rhythmicity, their expression was also influenced

by factors other than direct effects of light. Overall, misalignment between light and temperature cycles did not disrupt oscillations of putative core clock genes. *Clock*, *Helt*, and *PAR-bZIP-a* were among two dozen genes that did not shift in phase relative to the light cycle, while the phases of 3 putative repressors of CLOCK activity (*CIPC*, *Cry2*, and *PAR-bZIP-c*) advanced in phase by 5-8h under SC. If any of these genes do in fact regulate clock activity, their phase shifts could alter the timing of CLOCK-mediated transactivation activity, and thus downstream gene expression and behavior, without changing the expression of *Clock* itself.

Surprisingly, we found that *Clock* mRNA did not oscillate during a temperature cycle, although rhythmic behavior did occur (Fig. 2). *Clock* was one of only a few genes to be strictly in-phase with the light cycle during SC; also, *Clock* expression is induced by blue light and not green light, although green light drives normal rhythmic behavior [57]. Taken together, the evidence suggests that rhythmic *Clock* expression is entirely driven by (blue) light and is not required for rhythmic behavior. This raises questions about how *Nematostella* TTFL's are regulated by light and temperature. We are not aware of any other system in which *Clock* mRNA oscillates in response to one zeitgeber and not another (*Clock* oscillates during both light and temperature cycles in *Drosophila* [58] and fish [16, 59], and *Cycle/Bmal* does the same in mammals [60]), although circadian rhythms can persist when *Clock* cycling is genetically abolished in *Drosophila* [61]. The mechanisms by which light and temperature regulate *Clock* thus likely differ from bilaterian model systems. It is possible that *Clock* exhibits temperature-driven rhythms in a subset of cells, or that temperature acts on *Clock* activity at a level other than transcription. Strictly speaking, we do not even know whether *Clock* is required for circadian rhythms in *Nematostella*.

Global patterns of gene expression during SC

To our knowledge, this is the first study of transcriptome-wide gene expression during SC in any organism. Having observed that 12h SC resulted in the disruption of rhythmic locomotion, we had expected that, perhaps, *Nematostella* would simply have fewer rhythmic genes during SC. This would be consistent with circadian dysregulation in cavefish, which have evolved in arrhythmic environments and have fewer rhythmic transcripts than surface populations [62]. The imposition of arrhythmic feeding regimes also reduces the number of rhythmic transcripts in mouse liver [63]. However, we observed only slightly fewer rhythmic genes under SC (2440 vs. 2868), of which less than half were shared with rhythmic genes during aligned zeitgeber cycles. In other words, while many genes did lose rhythmicity during SC, several hundred genes in turn gained rhythmicity. It

is unclear whether the rhythmicity of most genes that uniquely cycle under SC is unimportant, deleterious, or serves some sort of homeostatic function; however, SC-specific genes had slightly lower mean expression than Align-specific genes. The phase distribution of circadian transcripts was bimodal during both aligned and SC conditions, as in many other systems (e.g. [62, 64–66]). Genes with phases during the two transcriptional "peaks" (ZT0-6 and ZT12-18) were less likely to lose rhythmicity during SC (38% lost rhythmicity compared to 53% of other genes; Chi-squared test, $p<2 \times 10^{-16}$), suggesting that rhythmic gene expression during these windows is somehow more robust.

Daily temperature cycles are much stronger regulators of gene expression than light cycles in *Nematostella*, in the sense that many more genes directly followed the phase of the temperature cycle than the light cycle. We were surprised that just 25 genes responded directly to light, given the strong acute effects of light on behavior. Our results are consistent with observations in *Drosophila* that a large portion of the transcriptome is directly regulated by diel temperature cycles, presumably an important response to short-term temperature variability for ectothermic animals [50]. However, it is possible that some temperature-responsive genes are not only directly driven by temperature, but are regulated through the clock. This is supported by the observation that the amplitude of temperature-responsive genes was reduced during SC. Additionally, temperature-responsive genes were enriched for transcription factor activity and metabolic processes such as autophagy, ABC transporter activity, and mRNA metabolism, all of which are processes known to be under clock control in other animals [67–69].

Circadian clocks are key regulators of metabolic homeostasis; this coordination of metabolic processes is generally considered adaptive because metabolite levels are optimized for periods of high and low energy demand throughout the day [67, 70]. Misalignment of light and temperature cycles caused substantial changes to the expression of genes that mediate cellular metabolism in *Nematostella*, which is likely to have bioenergetic consequences. For example, ribosome biogenesis is one of the most energy-intensive cellular processes [71] and is probably optimized by the circadian clock to occur when energy is most available [72]. Ribosomal genes in *Nematostella* were strongly rhythmic under aligned conditions and lost rhythmicity during SC. Genes related to endocytosis, vacuolar transport, and autophagy, which mediate protein and organelle degradation and are critical for cellular homeostasis [67, 73], maintained rhythmic expression during SC but shifted in phase by 12h. Since all animals were fed at the same time during the entrainment period, SC changed the timing of these processes in relation to feeding, and thus the period of peak energy availability

(animals were not fed for 48h during the sampling time points, so the observed gene expression patterns were not directly affected by time of feeding). We also observed a 12h phase shift for mitophagy genes; mitophagy regulates the number of mitochondria in response to cellular energy requirements [74], so changes in mitophagy could affect mitochondrial function and respiration. Finally, genes related to glucose metabolism gained rhythmic expression during SC, suggesting that clock dysregulation altered the expression of glucose regulatory genes. Both mitophagy and gluconeogenesis are impaired in mammalian clock knockout models [75]. In general, metabolic and circadian regulatory networks are tightly connected, and *Nematostella* clearly experienced dramatic perturbations to metabolic gene expression during SC. Although we only measured mRNA expression here, the downstream activity of processes like autophagy and ribosome biogenesis are controlled, at least in part, by rhythmic transcript expression [72, 76]. The potential disruption of metabolic homeostasis during SC could have deleterious consequences for *Nematostella*. Changing time of feeding to conflict with circadian rhythms can negatively impact reproductive fitness [77], and disruption of clock function (through knockouts or environmental perturbations) is linked to various metabolic diseases in the context of mammalian models and human health (e.g. [78–81]).

It is important to keep in mind that RNA abundance is a steady-state product of transcription and degradation. As such, rhythmic RNA levels can be produced by rhythmic transcription, rhythmic degradation, or both [82]. In fact, post-transcriptional regulation may be critical for the rhythmic expression of most genes: in mammals, more than 70% of mRNAs with rhythmic expression are not rhythmically transcribed [83]. Clocks can mediate RNA editing and splicing [69], and temperature rhythms are also associated with alternative splicing programs [84]. Consistent with this, we observed changes to genes that mediate RNA metabolism, including the spliceosome. Therefore, gain or loss of rhythmic mRNA expression could be caused by rhythmic variation in splicing, polyadenylation, regulation by microRNAs, or any other post-transcriptional process [85]. Similarly, RNA expression of core clock genes is only one snapshot of a multi-level process that forms the TTFL, with post-transcriptional regulation, protein expression, and post-translational regulation all playing critical roles in the regulation and output of molecular clocks [44, 45, 86]. Protein turnover is a major process subject to circadian regulation [87], and the loss of rhythmic expression of ribosomal genes and translation initiation factors, in conjunction with changes to autophagy and proteasome components, likely has wide-ranging effects on global protein expression and could alter the expression of proteins that are not themselves regulated by the clock.

Co-expression network analysis revealed that higher-order relationships between rhythmic genes

were also affected by SC. Although the underlying co-expression network structure was somewhat preserved (meaning that genes with correlated expression under aligned conditions tended to remain correlated with one other during SC), rhythmic genes were much less well-correlated to one another during SC overall, and eigengene expression explained less of rhythmic expression variance. Thus, SC weakened the relationships between rhythmic genes. Network analyses confirmed that temperature cycles were the dominant driver of rhythmic gene expression, as the only modules to maintain strong rhythmicity during both aligned and SC conditions all followed the phase of the temperature cycle (no module was strongly rhythmic in both conditions and shifted in phase by less than 10 hours).

Subsets of genes that may normally peak in expression at the same time of day respond differently to SC, indicating different modes of regulation and divergent responses to environmental stimuli. This is illustrated by the fact that some co-expression modules in the Aligned network were "split" into multiple modules in the Full network (e.g. Blue-A; Fig. 6c). Some modules identified across normal and disrupted clock conditions were enriched for putative binding motifs, suggesting regulation by shared mechanisms. Promoters of the Green-F module, containing Clock, were enriched for putative binding motifs with unknown function. This module lost rhythmicity under SC, meaning that although Clock itself maintained rhythmic expression, many genes co-expressed with Clock did not. The Brown-F module was expressed in antiphase to Green-F under aligned conditions and contained CIPC and PAR-bZIP-c, which are putative negative regulators of Clock activity. The largest module, Turquoise-F, was enriched for autophagy genes. Promoters of both Brown-F and Turquoise-F were enriched for bZIP binding motifs; bZIP motifs were also enriched among the promoters of genes that were rhythmic in both aligned and SC condition, and various groups of genes identified in our differential expression analysis. Therefore, binding by bZIP transcription factors may regulate the transcription of multiple groups of rhythmic genes. PAR-bZIP proteins regulate clock output pathways in both mammals [88] and *Drosophila* [89] (where they are necessary for rhythmic locomotor activity), but are not necessary for function of the clock itself [61]. Promoters of other modules were enriched for HTH motifs (an extremely broad class of DNA-binding domains [90]), ETS motifs (a type of HTH motif [91]), and SOX motifs. SOX genes are involved in circadian regulation in mammals, where SOX2 is necessary for light entrainment and locomotor rhythms [92]. In our data, a *Nematostella* SOX gene annotated as a Sox2 (NVEC200_010205) was rhythmic and shifted in phase by 12h (S2 Table). In summary, bZIP, and possibly SOX, family transcription factors may regulate circadian gene expression in *Nematostella*, in addition to bHLH transcription factors such as *Clock*, *Cycle*, and *Helt*.

Enrichment analysis also identified modules that appear to mediate processes known to play roles in bilaterian circadian rhythms. This includes chromatin organization (Black-F module, [93]), purine metabolism (Purple-F module, [94, 95]), and oxidoreductase activity (Magenta-F module, [96]). Green-F genes were enriched for GO terms related to protein transport, RNA metabolism, and methyltransferase and histone activity, suggesting roles in the regulation of gene expression (Clock itself is a histone acetyltransferase [97]). Broadly speaking, many processes under circadian control in bilaterian animals are also rhythmically expressed, and in many cases perturbed by SC, in *Nematostella*. This is perhaps unsurprising because nearly all cellular processes are connected to circadian rhythms in some way.

What causes sensory conflict?

Although we are limited by lack of knowledge of the molecular pathways that mediate light and temperature inputs and control locomotion in *Nematostella*, one possible framework for understanding disruption of circadian rhythms by SC is that clocks in different tissues respond differently to light and temperature. In bilaterians, it is tempting to imagine that differential responses of central and peripheral clocks to zeitgebers underlie clock disruptions, as these clocks can differ in their responses to SC when considered separately [4, 22]. We found that SC disrupts organism-level behavior in an animal without a brain, meaning that it is not necessary to invoke desynchronization of central and peripheral clocks to explain SC. However, we do not suggest that *Nematostella* are simple or homogeneous at the tissue level: they certainly have, for instance, many different neuronal subtypes [98], and may possess spatially distinct clocks in different cells. In fact, such heterogeneity exists within *Drosophila* central clocks, where distinct neuron populations have different sensitivities to light and temperature [21]. Although desynchronization of tissue-specific oscillators may well contribute to organism-level effects of SC, dissociation of clock gene expression can occur even within single cells [99]. The broader question of whether behavioral disruptions result from disruption to individual clocks, or desynchronization between multiple clocks distributed throughout the body, remains.

Future directions

The use of two zeitgeber cycles introduces an explosion of possible experimental designs, so we had to make several choices related to the design of sensory conflict experiments. Although our experimental results support the choice to align the coldest point of the temperature cycle with

lights-on, the precise choice of a reference relationship between zeitgeber cycles is arbitrary because we lack prior knowledge of how the phase of a zeitgeber relates to the phase of the clock [4]. We also chose to release animals into the mean temperature, 20 °C, and it is possible that other free-running temperatures could influence behavior. For example, the temperature of release into free-running affects the phase of eclosion rhythms in flies [19]; we do not know whether an analogous phenomenon affects *Nematostella*'s behavioral rhythms. There is a great deal of room for future experiments to test specific manipulations of zeitgebers and their inter-relationships, including different temperature ranges, free-running temperatures, and relative times of release into free-running.

Our RNA-seq data provide a first look at gene expression responses to light and temperature cycles, but cannot distinguish transcriptomic changes due to the circadian clock from those caused by direct effects of temperature. It will be interesting in the future to specifically measure thermally-entrained gene expression rhythms, and free-running rhythms following sensory conflict. It is also likely that future single-cell studies will identify distinct rhythmic clock outputs across cnidarian tissues and cell types, and these may exhibit distinct responses different zeitgebers. Finally, there is a need to clarify the molecular architecture of the cnidarian circadian clock through functional studies in order to better understand how light and temperature interact to control gene expression and behavior.

Conclusion

Light and temperature cycles both entrain circadian locomotor behavior in *Nematostella vectensis*. When these two zeitgebers are in phase with one another, they act synergistically to drive robust nocturnal behavior, and nocturnal rhythms occur even when the phases of light and temperature cycles differ by up to 8h. However, when phases differ by 10-12h, behavior becomes disrupted and arrhythmic on average. Some individuals maintain circadian behavior even under extreme sensory conflict, but their phases are not synchronized. These data provide a first look at how the circadian clock of a non-bilaterian animal integrates information from multiple zeitgebers, and show that neither light nor temperature is a totally dominant entraining cue. After weeks of exposure to sensory conflict, the transcriptome showed several signatures of disrupted rhythmic gene expression, including gain and loss of rhythmic genes and the weakening of co-expression patterns. Overall, temperature was a much stronger driver of gene expression than light in our study. It seems that, rather than simply reducing the number of rhythmic transcripts, sensory conflict causes turnover in

the identities of rhythmic genes and alters the relative timing of expression between them; these changes lead to the disruption of co-expressed, functionally related groups of genes, and ultimately to disrupted behavior at the organismal level.

Materials and methods

Animal culture

Animals used in this study were adult anemones of mixed sex. The laboratory population was originally collected from Great Sippewissett Marsh, MA USA and maintained in the laboratory for several generations. *Nematostella* were kept in glass water dishes containing half-strength 1 µm-filtered seawater (from Buzzards Bay, MA), diluted 1:1 with distilled water to a salinity of approximately 16. Water was changed weekly. Prior to acclimating to experimental conditions, anemones were kept at room temperature (18 °C) and fed brine shrimp nauplii four times per week.

Behavioral experiments

Anemones were acclimated within an incubator to the appropriate light and temperature regime for a given experiment for a minimum of two weeks prior to behavioral monitoring. They fed as described in the previous section during the acclimation period, but not during behavioral monitoring. A schematic of the experimental design is given in Fig. 1.

In the first set of experiments, *Nematostella* were kept in gradually changing (ramped) 24h temperature cycles in constant darkness. To produce the temperature cycle, the incubator was programmed such that the water temperature (not the air temperature) reached the desired temperature on the hour, which was monitored with HOBO temperature loggers. Some experiments were performed with a 14–26 °C temperature cycle (changing by 1 degree per hour), and some with an 8–32 °C temperature cycle (2 degrees per hour). We defined the coldest point of the temperature cycle as ZT0. For the 14–26 °C cycle, ZT0 occurred at 6am EST, or 7am EDT. For the 8–32 °C cycle, ZT0 occurred at 3am EST. Animals were fed with the aid of a dim red-light headlamp (*Nematostella* behavior is most sensitive to blue light and least sensitive to red light [41, 57]).

Acclimation to sensory conflict (SC) experiments was similar, except that the incubator was also programmed with a 12:12 light-dark cycle. All SC experiments used the 14–26 °C temperature cycle. The main population of anemones was maintained in an incubator with an "aligned" light and temperature cycle, such that ZT0 corresponded to lights-on and the coldest part of the temperature

cycle. ZT0 occurred at 6am EST/7am EDT. For other experimental groups, anemones were transferred from the aligned incubator to a second incubator where the temperature cycle was shifted by some amount relative to the light cycle. Therefore, each experimental group in the SC experiments was maintained in aligned light and temperature cycles prior to acclimating to the SC experimental conditions. In addition to the aligned cycles, we tested 6 light and temperature regimes in which the phase of the temperature cycle was delayed relative to the light cycle in a 2-h increment. The 7 experimental regimes were: aligned, 2-h offset, 4-h offset, 6-h offset, 8-h offset, 10-h offset, and 12-h offset. For these experiments, ZT0 always corresponds to lights-on, so the phase of the temperature cycle is defined relative to the light cycle. For instance, a 6-h offset means that the coldest point of the temperature cycle occurred at ZT6 (Fig. 1b). Behavioral monitoring (below) was performing during both cycling and free-running conditions, resulting in a total of 14 experimental groups each with n=24 anemones (one group had n=36).

After acclimating to the experimental conditions, behavior was monitored using Noldus Daniovision observation chambers equipped with infrared-sensitive cameras (DVOC-0040, Noldus Information Technology). Anemones were fed the day before each behavioral trial. A few hours after feeding, 12 anemones were transferred to individual wells of two 6-well plates and left in the incubator overnight. This was done to avoid directly handling the animals at the start of the experiment. At the start of each trial, the 6-well plates were placed into two Noldus chambers. In order to control the temperature during behavioral monitoring, a custom flow-through water system was constructed. A separate tank was heated and cooled using an aquarium heater and cooler connected to a programmable temperature controller. This water was then flowed around the plate inside the observation chamber using aquarium pumps, and water temperature was monitored with iButton temperature loggers. As before, the temperature controller was programmed such that the water temperature, not air temperature, reached the correct temperature at the correct time.

During the temperature cycle experiments, animals were transferred to the Noldus chambers at ZT6 (14–26 °C), or ZT8-10 (8–32 °C). Trial lengths ranged from 69-73 hours. For the 14–26 °C cycle, the free-running temperature was 20 °C, which was held constant beginning at ZT6. For the 8–32 °C cycle, the free-running temperature was 24 °C, beginning at ZT8.

For the sensory conflict experiments, each trial began at ZT6 (12pm EST/1pm EDT), and was recorded for 78 h. For free-running trials, the free-running period began at ZT12, 6 h after the start of recording; these time series thus had a length of 72 h. It was necessary to release groups into constant temperature (20 °C) at different times because the relationship between light and temperature cycles

was different for each group (see Fig. 1b; the beginning of free-run *per se*, meaning lights-off and 20 °C, was the same for every group). This was necessary to avoid sudden jumps in temperature, and a similar approach was used in [22]. Videos were recorded with a framerate of 2 frames per second.

qRT-PCR

Anemones were maintained in a 8–32 °C temperature cycle in constant darkness (as described above) and sampled every 4 h over 48 h (13 time points), beginning at ZT12 (3pm EST). In parallel, another group of animals was moved to constant temperature (24 °C) at ZT8 (11:00 h) and were then sampled at the same time points as the cycling group (ZT12, etc.). Four biological replicates were sampled at each time point, and each replicate consisted of three pooled individuals. Total RNA was extracted using the Aurum Total RNA Fatty and Fibrous Tissue Kit (Bio-Rad) following the manufacturer's protocol with DNAse treatment. RNA quality and concentration was checked with a NanoDrop spectrophotometer. Any libraries with low 260/230 ratios (< 1.8) or low concentration were re-purified using a Zymo RNA Clean and Concentrator kit. All RNA libraries were then diluted to 20 ng µL^{-1} and reverse transcription was performed with an iScript cDNA synthesis kit (Bio-Rad).

Primers for five genes—*Clock*, *Cry1a*, *Cry1b*, *Cry2*, and *Helt*—were ordered from Thermo Fisher and diluted to a working concentration of 10 µM. Primer sequences are given in Table A in S1 Appendix. Quantitative PCR (qPCR) was performed with iTaq Universal SYBR Green Supermix. The 20 µL reaction mixture was as follows: 10 µL Supermix, 8 µL nuclease-free water, 1 µL cDNA, and 0.5 µL each of forward and reverse primers. All samples for a given prier pair were performed on a single 96-well plate. Annealing temperatures were tested with a gradient for each primer pair followed by a melt curve analysis. 60 °C was chosen as the annealing temperature because it resulted in the lowest C_q values with specific amplification. The thermocycler was programmed as follows: 95 °C for 3 min, 40 cycles of 95 °C for 10 s and 60 °C for 30 s, followed by a melt curve analysis.

Quantitative PCR data analysis was performed with LinRegPCR [100], which estimates starting cDNA quantities by regressing the log-linear phase of the PCR curve. We excluded a total of three samples from further analysis because several genes failed to amplify. Gene expression was normalized using the NORMA-Gene algorithm [101]. Rhythmicity was tested with Lomb-Scargle periodograms (LSP) implemented in the R package 'lomb' v2.0, with periods between 20-28 h. Significance was assessed with n=2000 permutations, with a slight modification to the default

'randlsp' command. Since each time point contained replicates, all 49 data points (3-4 replicates x 13 time points) were shuffled, and then the mean time point values were re-calculated for the permuted data. In contrast, the default behavior of 'randlsp' is to simply shuffle the original mean time points.

RNA extraction and sequencing

Anemones were either maintained in aligned light and 14–26 °C temperature cycles, or with the temperature cycle offset by 12h (Fig. 1b). Animals were sampled every 4 h over 48 h (13 time points), beginning at ZT6. At each time point, animals were immediately preserved in RNA-later. Each time point contained three biological replicates of five pooled individuals each, with the exception of one library that consisted of three pooled individuals. This was because the initial 5-animal pool produced a low yield, so a new pool was constructed from 3 remaining animals from that treatment group. RNA was extracted using the Aurum Total RNA mini kit. We followed the manufacturer's instructions, except we incubated the RNA lysis buffer on ice for 30 min following tissue homogenization. Concentrations and quality were assessed with a Nandrop spectrophotometer and a Qubit fluorometer. Libraries were sequenced using 3' Tag-seq to give 100bp single-end reads at the UT Austin Genomic Sequencing and Analysis Facility (GSAF) on a NovaSeq 6000.

Data analysis, behavior

Animal coordinates were extracted from raw video files using the machine learning software DeepLabCut v2.1 (DLC, [102]). First, each raw video with footage of six individual anemones was cropped into six videos to be analyzed separately. Then a training dataset was constructed from 3699 images, in which we manually labelled the center-point of individual anemones. The DLC algorithm was trained on this dataset for 600,000 iterations. We used default settings, including the default neural networeads rk ("resnet_50"). DLC analysis outputs a file of XY coordinates for each video, with 2 frames per second. The files were analyzed using R code derived from the DLCAnalyzer Github package (https://github.com/ETHZ-INS/DLCAnalyzer, [103]); custom code used for this paper is available at this github repository: https://github.com/caberger1/Sensory-Conflict-in-Nematostella-vectensis. Frames with a likelihood less than 0.90 were removed and interpolated, as were frames where the recorded movement was more than 2 cm per frame. In order to reduce noise, an animal was considered "moving" if its speed was at least 0.03 $\mathrm{cm\,s^{-1}}$ for a period of at least 3 s (6 frames); any other movement was considered noise and ignored for downstream analysis. For

each animal, distance moved was summed into hourly bins based on real-world clock times and normalized to that animal's maximum hourly movement. This corrects for differences in overall activity due to e.g. body size (as in [37–39]). For each experimental group, we averaged the time points to produce a mean time series, which we analyzed alongside the individual time series. Time series were smoothed with a centered moving average in 4 h windows. In the case of mean time series, time points were first averaged, then smoothed.

Statistics

Two complementary rhythmicity tests were used. The first was a Lomb-Scargle periodogram (LSP) implemented within the R package 'lomb', with periods restricted from 20-28 hours and significance assessed by permutation (n=2000). In this case, the default 'randlsp' behavior was used. The second test, the empirical JTK method, was implemented within the BioDare2 web portal ('eJTK Classic'). This approach fits a series of cosinor waves with 24h periods, thus testing for periods of exactly 24h. The LSP test with periods restricted from 10-14h was also used to test for circatidal rhythms. In all cases, p-values were adjusted by Benjamin-Hochberg correction, and we chose a conservative FDR cutoff of 0.001 because we were only interested in time series that could confidently be identified as rhythmic.

The 'mFourFit' method implemented in the BioDare2 web portal was used to calculate periods and phases of time series. This is a curve-fitting procedure that is generally the most accurate of the available methods for short time series [104].

The R package 'CircaCompare' v0.1.1 was used to test for differences in amplitude and phase of mean time series. CircaCompare uses a cosinor curve-fitting approach and thus gives different estimates of phase and amplitude than those calculated by MFF; however, CircaCompare allows for formal hypothesis testing. The Rayleigh test for circular uniformity [105] was used to test whether groups of phases were distributed non-uniformly (implemented in the R package 'circular' v0.4). A bootstrapped version of Watson's non-parametric test (described in [106, 107] and implemented in the R package 'AS.circular' v0.0.0.9) was used to test whether phase distributions differed in their mean direction; significance was assessed with 9999 bootstraps. The Kruskal-Wallis test followed by Dunn's test for multiple comparisons were used to test for difference in non-circular means between groups (implemented in R packages 'stats' v4.0.3 and 'dunn.test' v1.3.5). Levene's test was used to test for differences in variance ('car' v3.0), and paired Wilcoxon rank tests ('stats' v4.0.3) were used to test for differences in the distance to expected light and temperature phases. Unless otherwise

noted, p-values were corrected for multiple testing using the Benjamini-Hochberg procedure.

For the purposes of calculating rhythmicity, we normalized the activity of each individual to its maximum hourly movement (see above). We also used linear mixed effects models to test for differences in un-normalized activity levels between groups, considering two measures of activity: percent time active, and total distance covered. Each hour of activity for each individual was considered a separate observation. In these models, we accounted for baseline differences in activity between individuals using random intercepts, and for autocorrelation of residuals using a correlation structure of AR(1); using more complex correlation structures did not affect the results. Mixed models were implemented in the R package 'nlme' v3.1, and post-hoc testing was done using 'emmeans' v1.6.2.

We performed time series clustering analysis by first decomposing smoothed mean time series using wavelet transformation in the R package 'biwavelet' v0.20.21, with the smallest scale (period) set to 2 and the largest scale to 36. We used the 'wclust' command to construct a distance matrix of the 14 wavelet series, and then performed a principal component analysis (PCA) on the distance matrix with 'FactoMineR' v2.4. We then performed hierarchical clustering on the principal components with the 'HCPC' command using complete linkage (Ward clustering gave identical results). Uncertainty in the clustering analysis was quantified with he pvclust v2.2 R package [108] with 1000 bootstraps, and clustering and PCA analyses were visualized with the 'factoextra' package v1.0.7.

Data analysis, gene expression

Raw reads were trimmed using Cutadapt v3.3 [109] with a minimum length of 25 and quality cutoff of 5, and mapped to the Simrbase Nvec200_v1 genome [110] using Salmon v1.5.1 with "selective alignment (full)" (SAF) [111], a k-mer size of 21, and no length correction (as Tag-seq reads do not have length bias). With SAF, the genome is used as a decoy, such that reads that better map to non-coding genomic sequences rather than coding sequences are discarded. Tximport v1.16.1 [112] was used to import counts into R; counts were then TMM-normalized [113] and expressed as counts per million on a log2 scale. Raw reads from [38] and [39] were re-analyzed in the same way as above, except they were length-corrected. Differential expression (DE) analysis was performed using limma-voom 3.44.3

Rhythmic gene expression was tested using RAIN (rhythmicity analysis incorporating nonparametric methods, [52]) v1.24.0. Search was performed for waveforms with a period of 24 h and

asymmetries in 4 h increments. P-values were corrected using the Bonferroni procedure, and a cutoff of $p<0.01$. Phases and amplitudes of rhythmic genes were calculated using CircaCompare. Rao's two-sample test for homogeneity [114] was used to test whether groups of phases were drawn from the same underlying distribution (implemented in the R package 'TwoCircular' v1.0), and significance was assessed with 10,000 Monte-Carlo replications. Discriminant analysis of principal components was conducted with the R library 'adegenet' v2.1.4 and code modified from [115].

Gene ontology enrichment analysis was performed with the GO_MWU R package with default settings (`https://github.com/z0on/GO_MWU`, [116]). GO annotations were downloaded from the SimrBase website (`https://simrbase.stowers.org/analysis/294`, NVEC200.20200813.gff). KEGG enrichment was performed with 'clusterProfiler' v3.0.4. Since genes in the SimrBase genome were not annotated with KEGG pathways, protein sequences from a previous *Nematostella* genome assembly (Nvec1, JGI) were downloaded from the KEGG website (`https://www.genome.jp/kegg/`) and queried against the SimrBase transcriptome using TBLASTN. SimrBase genes were annotated with the KEGG term of their best-scoring hit in each pathway, using an e-value cutoff of 1×10^{-10} and requiring >75% sequence identity. Sliding window enrichment analysis was performed to identify GO and KEGG terms enriched at certain times of day in each treatment. P-values were calculated (using GO_MWU for GO, and clusterProfiler for KEGG) by comparing genes with a phase within a 4h sliding window (e.g. ZT0-4, ZT3-6) against all other genes. The enrichment score of a gene at each of 24 hourly bins was then calculated by averaging the -log10 adjusted p-values from the 3 sliding windows that overlap the time point (e.g., the score for a gene at ZT3 would average the sliding windows ZT0-4, ZT1-5, and ZT2-6), and a gene was considered significantly enriched if the average score at any time point was greater than -log10(0.05).

Weighted Gene Co-expression Network Analysis v1.70 (WGCNA, [117]) was used to cluster rhythmic genes. For the full network constructed from all genes rhythmic in either time series, a soft-thresholding power of 5 was used, and a power of 8 was used for both the Align- and SC-specific networks. In all cases, a signed hybrid adjacency matrix, a minimum module size of 20, biweight midcorrelation ("bicor"), maxPOutliers=0.2, and mergeCutHeight=0.25 were used. Modules were analyzed for GO and KEGG enrichment as above. Rhythmicity of module eigengenes was assessed using LSP's with significance assessed via permutation (n=2000, periods 20-28). A linear model was used to correlate eigengene expression with light, temperature, and time. Module preservation statistics were calculated within the WGCNA package, and a Sankey plot was constructed using the package 'networkD3' v0.4. Enriched GO terms were calculated for each WGCNA module using

GO_MWU with module membership ('kME') as input and all other genes as background. KEGG enrichment was performed using a hypergeometric test within 'clusterProfiler', as above.

Putative promoter sequences 1kb upstream of transcription start sites were searched for potential enriched binding motifs using the HOMER motif discovery tool (findMotifs.pl), searching for motifs of lengths 6, 8, 10, and 12, retaining the top 15 motifs, and using all other promoters as background. Motifs were considered enriched at a p-value of 1×10^{-5} for "known" motifs, or 1×10^{-10} for *de novo* motifs.

Supporting information

S1 Appendix. Supplementary tables, figures, and text.

S1 Table. Behavioral rhythmicity results.

S2 Table. Differential expression, rhythmicity, and WGCNA analyses, and gene annotations.

S3 Table. GO and KEGG enrichment results.

S4 Table. Results of HOMER motif enrichment analyses.

S5 Table. Counts matrix. Contains TMM-normalized counts-per-million on a log2 scale.

Acknowledgments

We are particularly grateful to Dr. Carolyn Tepolt for generously providing the aquarium heater, cooler, and temperature controllers, and Dr. Kirstin Meyer-Kaiser for use of her incubator. We also thank Drs. Gregory Fournier, Casey Dunn, Carolyn Tepolt, and Yisrael Schnytzer for helpful discussions.

Data availability

Raw RNA-seq data have been uploaded to the NCBI Sequence Read Archive (SRA), Bioproject PRJNA826898. R code used for analysis is available at `https://github.com/caberger1/Sensory-Conflict-in-Nematostella-vectensis`.

References

1. Aschoff J. Exogenous and Endogenous Components in Circadian Rhythms. Cold Spring Harbor Symposia on Quantitative Biology. 1960;25:11–28. doi:10.1101/SQB.1960.025.01.004.

2. Salter MG, Franklin KA, Whitelam GC. Gating of the Rapid Shade-Avoidance Response by the Circadian Clock in Plants. Nature. 2003;426(6967):680–683. doi:10.1038/nature02174.

3. Fowler SG, Cook D, Thomashow MF. Low Temperature Induction of Arabidopsis CBF1, 2, and 3 Is Gated by the Circadian Clock. Plant Physiology. 2005;137(3):961–968. doi:10.1104/pp.104.058354.

4. Harper REF, Dayan P, Albert JT, Stanewsky R. Sensory Conflict Disrupts Activity of the Drosophila Circadian Network. Cell Reports. 2016;17(7):1711–1718. doi:10.1016/j.celrep.2016.10.029.

5. Rivas GBS, Bauzer LGSdR, Meireles-Filho ACA. "The Environment Is Everything That Isn't Me": Molecular Mechanisms and Evolutionary Dynamics of Insect Clocks in Variable Surroundings. Frontiers in Physiology. 2016;6. doi:10.3389/fphys.2015.00400.

6. Somers J, Harper REF, Albert JT. How Many Clocks, How Many Times? On the Sensory Basis and Computational Challenges of Circadian Systems. Frontiers in Behavioral Neuroscience. 2018;12. doi:10.3389/fnbeh.2018.00211.

7. Eelderink-Chen Z, Bosman J, Sartor F, Dodd AN, Kovács ÁT, Merrow M. A Circadian Clock in a Nonphotosynthetic Prokaryote. Science Advances. 2021;7(2):eabe2086. doi:10.1126/sciadv.abe2086.

8. Yoshida T, Murayama Y, Ito H, Kageyama H, Kondo T. Nonparametric Entrainment of the in Vitro Circadian Phosphorylation Rhythm of Cyanobacterial KaiC by Temperature Cycle. Proceedings of the National Academy of Sciences of the United States of America. 2009;106(5):1648–1653. doi:10.1073/pnas.0806741106.

9. Somers DE, Webb AA, Pearson M, Kay SA. The Short-Period Mutant, Toc1-1, Alters Circadian Clock Regulation of Multiple Outputs throughout Development in Arabidopsis Thaliana. Development (Cambridge, England). 1998;125(3):485–494. doi:10.1242/dev.125.3.485.

10. Merrow M, Brunner M, Roenneberg T. Assignment of Circadian Function for the Neurospora Clock Gene Frequency. Nature. 1999;399(6736):584–586. doi:10.1038/21190.

11. Rence B, Loher W. Arrhythmically Singing Crickets: Thermoperiodic Reentrainment after Bilobectomy. Science. 1975;190(4212):385–387. doi:10.1126/science.1179217.

12. Holmström WF, Morgan E. Laboratory Entrainaient of the Rhythmic Swimming Activity of Corophium Volutator (Pallas) to Cycles of Temperature and Periodic Inundation. Journal of the Marine Biological Association of the United Kingdom. 1983;63(4):861–870. doi:10.1017/S0025315400071277.

13. Glaser FT, Stanewsky R. Temperature Synchronization of the Drosophila Circadian Clock. Current Biology. 2005;15(15):1352–1363. doi:10.1016/j.cub.2005.06.056.

14. Darnell MZ. Ecological Physiology of the Circadian Pigmentation Rhythm in the Fiddler Crab Uca Panacea. Journal of Experimental Marine Biology and Ecology. 2012;426–427:39–47. doi:10.1016/j.jembe.2012.05.014.

15. Evans KJ. Responses of the Locomotor Activity Rhythms of Lizards to Simultaneous Light and Temperature Cycles. Comparative Biochemistry and Physiology. 1966;19(1):91–103. doi:10.1016/0010-406x(66)90549-4.

16. Lahiri K, Vallone D, Gondi SB, Santoriello C, Dickmeis T, Foulkes NS. Temperature Regulates Transcription in the Zebrafish Circadian Clock. PLoS Biology. 2005;3(11). doi:10.1371/journal.pbio.0030351.

17. Hart DW, van Jaarsveld B, Lasch KG, Grenfell KL, Oosthuizen MK, Bennett NC. Ambient Temperature as a Strong Zeitgeber of Circadian Rhythms in Response to Temperature Sensitivity and Poor Heat Dissipation Abilities in Subterranean African Mole-Rats. Journal of Biological Rhythms. 2021;36(5):461–469. doi:10.1177/07487304211034287.

18. Miyasako Y, Umezaki Y, Tomioka K. Separate Sets of Cerebral Clock Neurons Are Responsible for Light and Temperature Entrainment of Drosophila Circadian Locomotor Rhythms. Journal of Biological Rhythms. 2007;22(2):115–126. doi:10.1177/0748730407299344.

19. Currie J, Goda T, Wijnen H. Selective Entrainment of the Drosophila Circadian Clock to Daily Gradients in Environmental Temperature. BMC Biology. 2009;7:49. doi:10.1186/1741-7007-7-49.

20. Watari Y, Tanaka K. Interacting Effect of Thermoperiod and Photoperiod on the Eclosion Rhythm in the Onion Fly, Delia Antiqua Supports the Two-Oscillator Model. Journal of Insect Physiology. 2010;56(9):1192–1197. doi:10.1016/j.jinsphys.2010.03.022.

21. Yoshii T, Hermann C, Helfrich-Förster C. Cryptochrome-Positive and -Negative Clock Neurons in Drosophila Entrain Differentially to Light and Temperature. Journal of Biological Rhythms. 2010;25(6):387–398. doi:10.1177/0748730410381962.

22. Harper REF, Ogueta M, Dayan P, Stanewsky R, Albert JT. Light Dominates Peripheral Circadian Oscillations in *Drosophila Melanogaster* During Sensory Conflict. Journal of Biological Rhythms. 2017;32(5):423–432. doi:10.1177/0748730417724250.

23. Rivas GBS, Teles-de-Freitas R, Pavan MG, Lima JBP, Peixoto AA, Bruno RV. Effects of Light and Temperature on Daily Activity and Clock Gene Expression in Two Mosquito Disease Vectors. Journal of Biological Rhythms. 2018;33(3):272–288. doi:10.1177/0748730418772175.

24. Kaniewska MM, Vaněčková H, Doležel D, Kotwica-Rolinska J. Light and Temperature Synchronizes Locomotor Activity in the Linden Bug, Pyrrhocoris Apterus. Frontiers in Physiology. 2020;11. doi:10.3389/fphys.2020.00242.

25. Firth BT, Kennaway DJ. Thermoperiod and Photoperiod Interact to Affect the Phase of the Plasma Melatonin Rhythm in the Lizard, Tiliqua Rugosa. Neuroscience Letters. 1989;106(1):125–130. doi:10.1016/0304-3940(89)90213-9.

26. Valenciano AI, Alonso-Gómez AL, Alonso-Bedate M, Delgado MJ. Effect of Constant and Fluctuating Temperature on Daily Melatonin Production by Eyecups from Rana Perezi. Journal of Comparative Physiology B, Biochemical, Systemic, and Environmental Physiology. 1997;167(3):221–228. doi:10.1007/s003600050068.

27. Moyer RW, Firth BT, Lennaway DJ. Effect of Variable Temperatures, Darkness and Light on the Secretion of Melatonin by Pineal Explants in the Gecko, Christinus Marmoratus. Brain Research. 1997;747(2):230–235. doi:10.1016/S0006-8993(96)01266-8.

28. Firth BT, Belan I, Kennaway DJ, Moyer RW. Thermocyclic Entrainment of Lizard Blood Plasma Melatonin Rhythms in Constant and Cyclic Photic Environments. American Journal of Physiology-Regulatory, Integrative and Comparative Physiology. 1999;277(6):R1620–R1626. doi:10.1152/ajpregu.1999.277.6.R1620.

29. Bruce VG. Environmental Entrainment of Circadian Rhythms. Cold Spring Harbor Symposia on Quantitative Biology. 1960;25:29–48. doi:10.1101/SQB.1960.025.01.005.

30. Lin n, Chou n, Huang n. Priority of Light/Dark Entrainment over Temperature in Setting the Circadian Rhythms of the Prokaryote Synechococcus RF-1. Planta. 1999;209(2):202–206. doi:10.1007/s004250050623.

31. Javier Sánchez-Vázquez F, Zamora S, Madrid JA. Light-Dark and Food Restriction Cycles in Sea Bass: Effect of Conflicting Zeitgebers on Demand-Feeding Rhythms. Physiology & Behavior. 1995;58(4):705–714. doi:10.1016/0031-9384(95)00116-Z.

32. Challet E, Solberg LC, Turek FW. Entrainment in Calorie-Restricted Mice: Conflicting Zeitgebers and Free-Running Conditions. American Journal of Physiology-Regulatory, Integrative and Comparative Physiology. 1998;274(6):R1751–R1761. doi:10.1152/ajpregu.1998.274.6.R1751.

33. Reierth E, Stokkan KA. Dual Entrainment by Light and Food in the Svalbard Ptarmigan (Lagopus Mutus Hyperboreus). Journal of Biological Rhythms. 1998;13(5):393–402. doi:10.1177/074873049801300504.

34. Lague M, Reebs SG. Phase-Shifting the Light–Dark Cycle Influences Food-Anticipatory Activity in Golden Shiners. Physiology & Behavior. 2000;70(1):55–59. doi:10.1016/S0031-9384(00)00246-8.

35. Simion P, Philippe H, Baurain D, Jager M, Richter DJ, Di Franco A, et al. A Large and Consistent Phylogenomic Dataset Supports Sponges as the Sister Group to All Other Animals. Current Biology. 2017;27(7):958–967. doi:10.1016/j.cub.2017.02.031.

36. Laumer CE, Gruber-Vodicka H, Hadfield MG, Pearse VB, Riesgo A, Marioni JC, et al. Support for a Clade of Placozoa and Cnidaria in Genes with Minimal Compositional Bias. eLife. 2018;7:e36278. doi:10.7554/eLife.36278.

37. Hendricks WD, Byrum CA, Meyer-Bernstein EL. Characterization of Circadian Behavior in the Starlet Sea Anemone, Nematostella Vectensis. PLOS ONE. 2012;7(10):e46843. doi:10.1371/journal.pone.0046843.

38. Oren M, Tarrant AM, Alon S, Simon-Blecher N, Elbaz I, Appelbaum L, et al. Profiling Molecular and Behavioral Circadian Rhythms in the Non-Symbiotic Sea Anemone *Nematostella Vectensis*. Scientific Reports. 2015;5:11418. doi:10.1038/srep11418.

39. Tarrant AM, Helm RR, Levy O, Rivera HE. Environmental Entrainment Demonstrates Natural Circadian Rhythmicity in the Cnidarian *Nematostella Vectensis*. The Journal of Experimental Biology. 2019;222(21):jeb205393. doi:10.1242/jeb.205393.

40. Reitzel AM, Tarrant AM, Levy O. Circadian Clocks in the Cnidaria: Environmental Entrainment, Molecular Regulation, and Organismal Outputs. Integrative and Comparative Biology. 2013;53(1):118–130. doi:10.1093/icb/ict024.

41. Reitzel AM, Behrendt L, Tarrant AM. Light Entrained Rhythmic Gene Expression in the Sea Anemone Nematostella Vectensis: The Evolution of the Animal Circadian Clock. PLOS ONE. 2010;5(9):e12805. doi:10.1371/journal.pone.0012805.

42. Leach WB, Reitzel AM. Transcriptional Remodelling upon Light Removal in a Model Cnidarian: Losses and Gains in Gene Expression. Molecular Ecology. 2019;28(14):3413–3426. doi:10.1111/mec.15163.

43. Dibner C, Schibler U, Albrecht U. The Mammalian Circadian Timing System: Organization and Coordination of Central and Peripheral Clocks. Annual Review of Physiology. 2010;72(1):517–549. doi:10.1146/annurev-physiol-021909-135821.

44. Partch CL, Green CB, Takahashi JS. Molecular Architecture of the Mammalian Circadian Clock. Trends in Cell Biology. 2014;24(2):90–99. doi:10.1016/j.tcb.2013.07.002.

45. Dubowy C, Sehgal A. Circadian Rhythms and Sleep in Drosophila Melanogaster. Genetics. 2017;205(4):1373–1397. doi:10.1534/genetics.115.185157.

46. Reitzel AM, Tarrant AM. Nuclear Receptor Complement of the Cnidarian Nematostella Vectensis: Phylogenetic Relationships and Developmental Expression Patterns. BMC Evolutionary Biology. 2009;9(1):230. doi:10.1186/1471-2148-9-230.

47. Gornik SG, Bergheim BG, Morel B, Stamatakis A, Foulkes NS, Guse A. Photoreceptor Diversification Accompanies the Evolution of Anthozoa. Molecular Biology and Evolution. 2021;38(5):1744–1760. doi:10.1093/molbev/msaa304.

48. Zhao WN, Malinin N, Yang FC, Staknis D, Gekakis N, Maier B, et al. CIPC Is a Mammalian Circadian Clock Protein without Invertebrate Homologues. Nature Cell Biology. 2007;9(3):268–275. doi:10.1038/ncb1539.

49. Brady AK, Snyder KA, Vize PD. Circadian Cycles of Gene Expression in the Coral, Acropora Millepora. PLOS ONE. 2011;6(9):e25072. doi:10.1371/journal.pone.0025072.

50. Boothroyd CE, Wijnen H, Naef F, Saez L, Young MW. Integration of Light and Temperature in the Regulation of Circadian Gene Expression in Drosophila. PLoS Genetics. 2007;3(4):e54. doi:10.1371/journal.pgen.0030054.

51. Jombart T, Devillard S, Balloux F. Discriminant Analysis of Principal Components: A New Method for the Analysis of Genetically Structured Populations. BMC genetics. 2010;11:94. doi:10.1186/1471-2156-11-94.

52. Thaben PF, Westermark PO. Detecting Rhythms in Time Series with RAIN. Journal of Biological Rhythms. 2014;29(6):391–400. doi:10.1177/0748730414553029.

53. De los Santos H, Collins EJ, Mann C, Sagan AW, Jankowski MS, Bennett KP, et al. ECHO: An Application for Detection and Analysis of Oscillators Identifies Metabolic Regulation on Genome-Wide Circadian Output. Bioinformatics. 2020;36(3):773–781. doi:10.1093/bioinformatics/btz617.

54. Weger BD, Gobet C, David FPA, Atger F, Martin E, Phillips NE, et al. Systematic Analysis of Differential Rhythmic Liver Gene Expression Mediated by the Circadian Clock and Feeding Rhythms. Proceedings of the National Academy of Sciences. 2021;118(3). doi:10.1073/pnas.2015803118.

55. Langfelder P, Luo R, Oldham MC, Horvath S. Is My Network Module Preserved and Reproducible? PLOS Computational Biology. 2011;7(1):e1001057. doi:10.1371/journal.pcbi.1001057.

56. Sachkova MY, Macrander J, Surm JM, Aharoni R, Menard-Harvey SS, Klock A, et al. Some like It Hot: Population-Specific Adaptations in Venom Production to Abiotic Stressors in a Widely Distributed Cnidarian. BMC Biology. 2020;18(1):121. doi:10.1186/s12915-020-00855-8.

57. Leach WB, Reitzel AM. Decoupling Behavioral and Transcriptional Responses to Color in an Eyeless Cnidarian. BMC Genomics. 2020;21(1):361. doi:10.1186/s12864-020-6766-y.

58. Glossop NRJ, Lyons LC, Hardin PE. Interlocked Feedback Loops Within the Drosophila Circadian Oscillator. Science. 1999;286(5440):766–768. doi:10.1126/science.286.5440.766.

59. Di Rosa V, Frigato E, López-Olmeda JF, Sánchez-Vázquez FJ, Bertolucci C. The Light Wavelength Affects the Ontogeny of Clock Gene Expression and Activity Rhythms in Zebrafish Larvae. PLOS ONE. 2015;10(7):e0132235. doi:10.1371/journal.pone.0132235.

60. Chun LE, Woodruff ER, Morton S, Hinds LR, Spencer RL. Variations in Phase and Amplitude of Rhythmic Clock Gene Expression across Prefrontal Cortex, Hippocampus, Amygdala, and Hypothalamic Paraventricular and Suprachiasmatic Nuclei of Male and Female Rats. Journal of Biological Rhythms. 2015;30(5):417–436. doi:10.1177/0748730415598608.

61. Gunawardhana KL, Hardin PE. VRILLE Controls PDF Neuropeptide Accumulation and Arborization Rhythms in Small Ventrolateral Neurons to Drive Rhythmic Behavior in Drosophila. Current biology: CB. 2017;27(22):3442–3453.e4. doi:10.1016/j.cub.2017.10.010.

62. Mack KL, Jaggard JB, Persons JL, Roback EY, Passow CN, Stanhope BA, et al. Repeated Evolution of Circadian Clock Dysregulation in Cavefish Populations. PLoS Genetics. 2021;17(7):e1009642. doi:10.1371/journal.pgen.1009642.

63. Greenwell BJ, Trott AJ, Beytebiere JR, Pao S, Bosley A, Beach E, et al. Rhythmic Food Intake Drives Rhythmic Gene Expression More Potently than the Hepatic Circadian Clock in Mice. Cell Reports. 2019;27(3):649–657.e5. doi:10.1016/j.celrep.2019.03.064.

64. Doherty CJ, Kay SA. Circadian Control of Global Gene Expression Patterns. Annual Review of Genetics. 2010;44(1):419–444. doi:10.1146/annurev-genet-102209-163432.

65. Le Martelot G, Canella D, Symul L, Migliavacca E, Gilardi F, Liechti R, et al. Genome-Wide RNA Polymerase II Profiles and RNA Accumulation Reveal Kinetics of Transcription and Associated Epigenetic Changes During Diurnal Cycles. PLOS Biology. 2012;10(11):e1001442. doi:10.1371/journal.pbio.1001442.

66. Li Y, Li G, Wang H, Du J, Yan J. Analysis of a Gene Regulatory Cascade Mediating Circadian Rhythm in Zebrafish. PLOS Computational Biology. 2013;9(2):e1002940. doi:10.1371/journal.pcbi.1002940.

67. Ma D, Li S, Molusky MM, Lin JD. Circadian Autophagy Rhythm: A Link between Clock and Metabolism? Trends in Endocrinology and Metabolism. 2012;23(7):319–325. doi:10.1016/j.tem.2012.03.004.

68. Pácha J, Balounová K, Soták M. Circadian Regulation of Transporter Expression and Implications for Drug Disposition. Expert Opinion on Drug Metabolism & Toxicology. 2021;17(4):425–439. doi:10.1080/17425255.2021.1868438.

69. Hardin PE, Panda S. Circadian Timekeeping and Output Mechanisms in Animals. Current Opinion in Neurobiology. 2013;23(5):724–731. doi:10.1016/j.conb.2013.02.018.

70. Thurley K, Herbst C, Wesener F, Koller B, Wallach T, Maier B, et al. Principles for Circadian Orchestration of Metabolic Pathways. Proceedings of the National Academy of Sciences. 2017;114(7):1572–1577. doi:10.1073/pnas.1613103114.

71. Warner JR. The Economics of Ribosome Biosynthesis in Yeast. Trends in Biochemical Sciences. 1999;24(11):437–440. doi:10.1016/s0968-0004(99)01460-7.

72. Jouffe C, Cretenet G, Symul L, Martin E, Atger F, Naef F, et al. The Circadian Clock Coordinates Ribosome Biogenesis. PLOS Biology. 2013;11(1):e1001455. doi:10.1371/journal.pbio.1001455.

73. Kocaturk NM, Gozuacik D. Crosstalk Between Mammalian Autophagy and the Ubiquitin-Proteasome System. Frontiers in Cell and Developmental Biology. 2018;6.

74. Li E, Li X, Huang J, Xu C, Liang Q, Ren K, et al. BMAL1 Regulates Mitochondrial Fission and Mitophagy through Mitochondrial Protein BNIP3 and Is Critical in the Development of Dilated Cardiomyopathy. Protein & Cell. 2020;11(9):661–679. doi:10.1007/s13238-020-00713-x.

75. de Goede P, Wefers J, Brombacher EC, Schrauwen P, Kalsbeek A. Circadian Rhythms in Mitochondrial Respiration. Journal of Molecular Endocrinology. 2018;60(3):R115–R130. doi:10.1530/JME-17-0196.

76. Ma D, Panda S, Lin JD. Temporal Orchestration of Circadian Autophagy Rhythm by C/EBPβ. The EMBO Journal. 2011;30(22):4642–4651. doi:10.1038/emboj.2011.322.

77. Xu K, DiAngelo JR, Hughes ME, Hogenesch JB, Sehgal A. The Circadian Clock Interacts with Metabolic Physiology to Influence Reproductive Fitness. Cell Metabolism. 2011;13(6):639–654. doi:10.1016/j.cmet.2011.05.001.

78. Turek FW, Joshu C, Kohsaka A, Lin E, Ivanova G, McDearmon E, et al. Obesity and Metabolic Syndrome in Circadian Clock Mutant Mice. Science (New York, NY). 2005;308(5724):1043–1045. doi:10.1126/science.1108750.

79. Green CB, Takahashi JS, Bass J. The Meter of Metabolism. Cell. 2008;134(5):728–742. doi:10.1016/j.cell.2008.08.022.

80. Nedeltcheva AV, Scheer FAJL. Metabolic Effects of Sleep Disruption, Links to Obesity and Diabetes. Current opinion in endocrinology, diabetes, and obesity. 2014;21(4):293–298. doi:10.1097/MED.0000000000000082.

81. Roenneberg T, Merrow M. The Circadian Clock and Human Health. Current biology: CB. 2016;26(10):R432–443. doi:10.1016/j.cub.2016.04.011.

82. Lück S, Thurley K, Thaben PF, Westermark PO. Rhythmic Degradation Explains and Unifies Circadian Transcriptome and Proteome Data. Cell Reports. 2014;9(2):741–751. doi:10.1016/j.celrep.2014.09.021.

83. Koike N, Yoo SH, Huang HC, Kumar V, Lee C, Kim TK, et al. Transcriptional Architecture and Chromatin Landscape of the Core Circadian Clock in Mammals. Science. 2012;338(6105):349–354. doi:10.1126/science.1226339.

84. Preußner M, Goldammer G, Neumann A, Haltenhof T, Rautenstrauch P, Müller-McNicoll M, et al. Body Temperature Cycles Control Rhythmic Alternative Splicing in Mammals. Molecular Cell. 2017;67(3):433–446.e4. doi:10.1016/j.molcel.2017.06.006.

85. Zhang R, Lahens NF, Ballance HI, Hughes ME, Hogenesch JB. A Circadian Gene Expression Atlas in Mammals: Implications for Biology and Medicine. Proceedings of the National Academy of Sciences. 2014;111(45):16219–16224. doi:10.1073/pnas.1408886111.

86. Jang C, Lahens NF, Hogenesch JB, Sehgal A. Ribosome Profiling Reveals an Important Role for Translational Control in Circadian Gene Expression. Genome Research. 2015;25(12):1836–1847. doi:10.1101/gr.191296.115.

87. Duffield GE, Best JD, Meurers BH, Bittner A, Loros JJ, Dunlap JC. Circadian Programs of Transcriptional Activation, Signaling, and Protein Turnover Revealed by Microarray Analysis of Mammalian Cells. Current Biology. 2002;12(7):551–557. doi:10.1016/S0960-9822(02)00765-0.

88. Gachon F. Physiological Function of PARbZip Circadian Clock-controlled Transcription Factors. Annals of Medicine. 2007;39(8):562–571. doi:10.1080/07853890701491034.

89. Cyran SA, Buchsbaum AM, Reddy KL, Lin MC, Glossop NRJ, Hardin PE, et al. Vrille, Pdp1, and dClock Form a Second Feedback Loop in the Drosophila Circadian Clock. Cell. 2003;112(3):329–341. doi:10.1016/s0092-8674(03)00074-6.

90. Aravind L, Anantharaman V, Balaji S, Babu MM, Iyer LM. The Many Faces of the Helix-Turn-Helix Domain: Transcription Regulation and Beyond⋆. FEMS Microbiology Reviews. 2005;29(2):231–262. doi:10.1016/j.fmrre.2004.12.008.

91. Liang H, Mao X, Olejniczak ET, Nettesheim DG, Yu L, Meadows RP, et al. Solution Structure of the Ets Domain of Fli-1 When Bound to DNA. Nature Structural Biology. 1994;1(12):871–875. doi:10.1038/nsb1294-871.

92. Cheng AH, Bouchard-Cannon P, Hegazi S, Lowden C, Fung SW, Chiang CK, et al. SOX2-Dependent Transcription in Clock Neurons Promotes the Robustness of the Central Circadian Pacemaker. Cell Reports. 2019;26(12):3191–3202.e8. doi:10.1016/j.celrep.2019.02.068.

93. Pacheco-Bernal I, Becerril-Pérez F, Aguilar-Arnal L. Circadian Rhythms in the Three-Dimensional Genome: Implications of Chromatin Interactions for Cyclic Transcription. Clinical Epigenetics. 2019;11(1):79. doi:10.1186/s13148-019-0677-2.

94. Fustin JM, Doi M, Yamada H, Komatsu R, Shimba S, Okamura H. Rhythmic Nucleotide Synthesis in the Liver: Temporal Segregation of Metabolites. Cell Reports. 2012;1(4):341–349. doi:10.1016/j.celrep.2012.03.001.

95. Li Y, Li G, Görling B, Luy B, Du J, Yan J. Integrative Analysis of Circadian Transcriptome and Metabolic Network Reveals the Role of De Novo Purine Synthesis in Circadian Control of Cell Cycle. PLOS Computational Biology. 2015;11(2):e1004086. doi:10.1371/journal.pcbi.1004086.

96. Johnson BP, Walisser JA, Liu Y, Shen AL, McDearmon EL, Moran SM, et al. Hepatocyte Circadian Clock Controls Acetaminophen Bioactivation through NADPH-cytochrome P450 Oxidoreductase. Proceedings of the National Academy of Sciences. 2014;111(52):18757–18762. doi:10.1073/pnas.1421708111.

97. Doi M, Hirayama J, Sassone-Corsi P. Circadian Regulator CLOCK Is a Histone Acetyltransferase. Cell. 2006;125(3):497–508. doi:10.1016/j.cell.2006.03.033.

98. Sebé-Pedrós A, Saudemont B, Chomsky E, Plessier F, Mailhé MP, Renno J, et al. Cnidarian Cell Type Diversity and Regulation Revealed by Whole-Organism Single-Cell RNA-Seq. Cell. 2018;173(6):1520–1534.e20. doi:10.1016/j.cell.2018.05.019.

99. Schmal C, Ono D, Myung J, Pett JP, Honma S, Honma KI, et al. Weak Coupling between Intracellular Feedback Loops Explains Dissociation of Clock Gene Dynamics. PLOS Computational Biology. 2019;15(9):e1007330. doi:10.1371/journal.pcbi.1007330.

100. Ruijter JM, Ramakers C, Hoogaars WMH, Karlen Y, Bakker O, van den Hoff MJB, et al. Amplification Efficiency: Linking Baseline and Bias in the Analysis of Quantitative PCR Data. Nucleic Acids Research. 2009;37(6):e45–e45. doi:10.1093/nar/gkp045.

101. Heckmann LH, Sørensen PB, Krogh PH, Sørensen JG. NORMA-Gene: A Simple and Robust Method for qPCR Normalization Based on Target Gene Data. BMC bioinformatics. 2011;12:250. doi:10.1186/1471-2105-12-250.

102. Mathis A, Mamidanna P, Cury KM, Abe T, Murthy VN, Mathis MW, et al. DeepLabCut: Markerless Pose Estimation of User-Defined Body Parts with Deep Learning. Nature Neuroscience. 2018;21(9):1281–1289. doi:10.1038/s41593-018-0209-y.

103. Sturman O, von Ziegler L, Schläppi C, Akyol F, Privitera M, Slominski D, et al. Deep Learning-Based Behavioral Analysis Reaches Human Accuracy and Is Capable of Outperforming Commercial Solutions. Neuropsychopharmacology. 2020;45(11):1942–1952. doi:10.1038/s41386-020-0776-y.

104. Zielinski T, Moore AM, Troup E, Halliday KJ, Millar AJ. Strengths and Limitations of Period Estimation Methods for Circadian Data. PLOS ONE. 2014;9(5):e96462. doi:10.1371/journal.pone.0096462.

105. Rayleigh L. XII. *On the Resultant of a Large Number of Vibrations of the Same Pitch and of Arbitrary Phase*. The London, Edinburgh, and Dublin Philosophical Magazine and Journal of Science. 1880;10(60):73–78. doi:10.1080/14786448008626893.

106. Fisher NI, Lewis T, Embleton BJJ. Statistical Analysis of Spherical Data. Cambridge University Press; 1993.

107. Pewsey A, Neuhäuser M, Ruxton GD. Circular Statistics in R. OUP Oxford; 2013.

108. Suzuki R, Shimodaira H. Pvclust: An R Package for Assessing the Uncertainty in Hierarchical Clustering. Bioinformatics. 2006;22(12):1540–1542. doi:10.1093/bioinformatics/btl117.

109. Martin M. Cutadapt Removes Adapter Sequences from High-Throughput Sequencing Reads. EMBnetjournal. 2011;17(1):10–12. doi:10.14806/ej.17.1.200.

110. Zimmermann B, Robb SMC, Genikhovich G, Fropf WJ, Weilguny L, He S, et al.. Sea Anemone Genomes Reveal Ancestral Metazoan Chromosomal Macrosynteny; 2020.

111. Srivastava A, Malik L, Sarkar H, Zakeri M, Almodaresi F, Soneson C, et al. Alignment and Mapping Methodology Influence Transcript Abundance Estimation. Genome Biology. 2020;21(1):239. doi:10.1186/s13059-020-02151-8.

112. Soneson C, Love MI, Robinson MD. Differential Analyses for RNA-Seq: Transcript-level Estimates Improve Gene-Level Inferences. F1000Research. 2016;4. doi:10.12688/f1000research.7563.2.

113. Robinson MD, McCarthy DJ, Smyth GK. edgeR: A Bioconductor Package for Differential Expression Analysis of Digital Gene Expression Data. Bioinformatics. 2010;26(1):139–140. doi:10.1093/bioinformatics/btp616.

114. Jammalamadaka SR, Guerrier S, Mangalam V. A Two-sample Nonparametric Test for Circular Data– Its Exact Distribution and Performance. Sankhya B. 2021;83(1):140–166. doi:10.1007/s13571-020-00244-9.

115. Dixon GB, Davies SW, Aglyamova GA, Meyer E, Bay LK, Matz MV. CORAL REEFS. Genomic Determinants of Coral Heat Tolerance across Latitudes. Science (New York, NY). 2015;348(6242):1460–1462. doi:10.1126/science.1261224.

116. Wright RM, Aglyamova GV, Meyer E, Matz MV. Gene Expression Associated with White Syndromes in a Reef Building Coral, Acropora Hyacinthus. BMC Genomics. 2015;16(1):371. doi:10.1186/s12864-015-1540-2.

117. Langfelder P, Horvath S. Eigengene Networks for Studying the Relationships between Co-Expression Modules. BMC Systems Biology. 2007;1:54. doi:10.1186/1752-0509-1-54.